MASTER'S THESIS OF NATURAL SCIENCE

Application of Push-Drift-Pull Tracer Tests at a CO_2 Storage Environmental Test Site and Identification of Factors Affecting Breakthrough Curves

이산화탄소 지중 저장 부지 수리특성화를 위한 Push-Drift-Pull 추적자 실험의 적용과 농도 이력 곡선에 영향을 주는 인자 파악

February 2017

Graduate School of Seoul National University

College of Natural Science

School of Earth and Environmental Sciences

KIM, HONG HYUN

ABSTRACT

A single well push-drift-pull tracer test is a convenient and cost-effective tool to characterize hydrogeological features of the subsurface aquifer system although it has a limitation on the tested results by various experimental designs. In this study, application of the single well push-drift-pull tracer test at the carbon capture and storage (CCS) environmental monitoring field site was performed for deciding suitable location of monitoring wells prior to the CO_2 leakage experiments. Laboratory-scale push-pull experiments with numerical simulation were also conducted to evaluate the factors affecting the result of push-drift-pull test and to suggest a proper test design for obtaining reliable results from the push-pull test.

By applying the single well push-pull tracer tests at the field with two tracers (salt and SF_6), local-scale estimates of the hydraulic properties (linear velocity, effective porosity) of the aquifer were obtained at the study site. Mass recovery percentage of the volatile tracer (SF_6) was lower than that of the non-volatile tracer (salt) and degassing of SF_6 was seemed to be intensified as drift time increased. Based on the obtained hydraulic properties and tracer mass recovery rates, an effective CO_2 monitoring network including unsaturated zone boreholes was installed at the study site.

To discover the affecting factors on the results of the push-drift-pull test, a series of laboratory-scale push-drift-pull tests were conducted with a sand tank under various controlled conditions such as variable drift time, tracer density, hydraulic gradient, and well penetrating depth. The results of the sensitivity analysis from the laboratory-scale tests presented the importance of sampling interval in most conditions except the penetrating depth. Several linear velocities were computed from the numerical simulation to investigate the effect of tracer density and pumping rate. The linear velocity was underestimated when input tracer concentration was increased because solute travel distance and direction during drift time were

dependent on the density of tracer plume. For the pulling phase, reasonable pumping rate must be applied to extract the majority of injected tracer mass in order to obtain reliable center of mass time (t_{com}) and analyze solute transport properties. Therefore, the factors that affect test results should be considered carefully to design a push-drift-pull tracer test.

Key words: push-drift-pull tracer test, multiple tracer test, effective CO_2 monitoring network, tracer test design

TABLE OF CONTENTS

LIST OF FIGURES

LIST OF TABLES

1 INTRODUCTION

1.1 Background

CO_2 monitoring system at shallow groundwater

The concern of global warming has been accelerated recently as a result of human activities involved with carbon-rich fossil fuels. One of the major contributors causing the global warming and greenhouse effect is the increased concentration of CO_2 (IPCC, 2007). To reduce atmospheric concentration of CO_2, many countries have been making an effort to develop technology. One of the technologies that can mitigate global warming is to capture CO_2 and store it into deep subsurface formations (IPCC, 2005). When CO_2 is injected into deep subsurface formations, there is a possibility that those injected CO_2 could escape from the reservoir and float up to the surface through flow channel like a fracture of formation or constructed borehole. If CO_2 leaking is prolonged, it can affect the chemical composition of groundwater, and various hazardous constituents will be released to groundwater (Kharaka et al., 2006; Zheng et al., 2009; Humez et al., 2013). Therefore, it is important to detect leaking CO_2 early and monitor the impacts caused by CO_2 storage at CCS (Carbon Capture and Storage) site.

Recently, the shallow-depth controlled CO_2 release facilities have been installed around the world for studying the hydrogeochemical impacts on groundwater and/or the influences on soil and atmospheric conditions (Kharaka et al., 2010; Cahill et al., 2014). The principal objectives of shallow groundwater monitoring using a controlled CO_2 release facility can be summarized as: 1) to identify whether groundwater is affected by the direct CO_2 leakage from the storage space or by the groundwater system change due to the CO_2 storage; 2) to demonstrate that the affected groundwater zone can be detected by the monitoring methods; 3) to identify which parameters should be included in the monitoring and how frequently each monitoring

parameter should be measured; and 4) to evaluate whether or not CO_2 leakage will change the groundwater quality to the extent causing health effects (Lee et al., 2016).

To make a huge effect for CO_2 leakage detection, proper position of observation boreholes for CO_2 monitoring should be situated at CCS monitoring site. In order to allocate the monitoring wells to predict transport of CO_2 plume, site characterization is one of important procedures to define hydraulic and geologic properties at the study site. According to previous studies, Peter et al. (2011) built the positions of CO_2 monitoring wells and well spacing along with groundwater flow direction. Ma et al. (2013) performed comprehensive geological and geophysical site characterization prior to constructing CCS monitoring network at Jinbian site. The injected solute into the subsurface aquifer system would flow to different aspect depending on the hydraulic properties of the aquifer, such as groundwater velocity and effective porosity. However, only a few studies considered the hydraulic properties derived from site characterization during building the CCS monitoring site.

A tracer test is a useful method for site characterizations to figure out a flow path of tracer on subsurface within a relatively short time, while understanding groundwater interaction and movement in the CCS study (Myers et al., 2013). A tracer test using noble gas such as Ar (Trautz et al., 2013) before the CO_2 injection and tracer injection such as SF_6 (Peter et al., 2012) together with CO_2 were performed at some test sites. There are many kinds of tracer tests using multi-well, including convergent tracer test, and dipole tracer test. However, single well push-drift-pull test is performed to determine various hydraulic properties of the aquifer system simply and economically (Istok, 2013) when one well is used for a tracer test.

Factors affecting the design of push-pull test results

Although the push-drift-pull tracer test has an advantage of easy to perform by using only

one tested borehole, hydraulic properties of the tested field or design conditions of the push-drift-pull test could cause misinterpretation of the aquifer properties. (Haggerty et al., 2000; Becker and shapiro, 2003; Hwang, 2004; Hebig et al., 2015). Haggerty et al. (2000) applied single well push-drift-pull tests to investigate the effect of rate-limited mass transfer (e.g., in dual porosity or multi porosity systems) on late-time behavior of tracer test breakthrough curves and found simple expression of late-time concentration. Becker and shapiro (2003) compared the transport parameters from various tracer experiment (radially convergent, weak-dipole, and push-pull), and they found out the dispersivity from the push-pull experiments was smaller than those obtained from the radially convergent experiment and weak-dipole tests. This is because conducting tracer experiments in a push-pull configuration removes the effect of hydrodynamic dispersion and heterogeneous advection from the breakthrough tail. Hwang (2004) performed the single well push-drift-pull tests under different conditions, altering extraction rate, drift time, hydraulic conductivity, and hydraulic gradient. He concluded that the mass recovery rate was inversely proportional to drift time, on the other hand hydraulic gradient was proportional to hydraulic conductivity. Hebig et al. (2015) conducted the single well push-drift-pull tests with different amount of chaser volume, and found out that chaser volume could affect the shape of breakthrough curve.

Even though there have been many laboratory experiments and field tests to investigate the factors affecting on push-drift-pull tests, other factors affecting the test result might exist that were not handled yet such as density effect of tracer.

1.2 Objectives and Scope

In this study, push-drift-pull tracer tests were performed to identify the hydraulic properties and investigate the influential factors.

First, the objectives of the field push-drift-pull test are to characterize hydrogeological characteristics at Eumseong EIT site and to build effective monitoring network at the CCS environmental test site. The tests were conducted at each screened interval of partial screened well to identify the hydraulic properties of each depth. Also, different drift times were applied to investigate the influence of drift time. Finally, situating monitoring wells to detect a CO_2 leakage efficiently based on evaluating behaviors of injected tracer at the study site.

Second, a laboratory push-drift-pull test has objectives to examine the impact of hydraulic properties and test conditions including density effect and pumping rate from the results of push-drift-pull tests. The sensitivity analysis was conducted to identify the effect of factors from the shape of breakthrough curves in time. In addition, the experimental results were used to validate a numerical model. Several numerical simulations were conducted under various density and pumping rate. The results of numerical simulations were used to assess the effect of density and pumping rate during estimating linear velocity. The results of laboratory push-drift-pull tests can help the design of optimizing single well push-drift-pull tracer test.

2 FIELD EXPERIMENT

2.1 Site Description

The study site is located in Eumseong, Chungcheongbuk-do (Fig. 2-1a), where monitoring environmental impact of CCS research is in progress by K-COSEM (Korea CO_2 Storage Environmental Management). The geological structure of the area mainly consists of coarse-grained gneissoid granite (Kang et al., 1980). The weathered zone is distributed to tens of meters from the surface due to highly weathered granite. Generalized geologic cross section (A-A') is showed in Fig. 2-2. Between the cross section A-A', ten boreholes were installed as full screened-wells with 30 m depth and diameter of 0.0508 m (BS-1, BS-2, BS-3, BS-4 and BS-5 in Fig. 2-1b). Four boreholes were constructed as partial-screened-wells (PS-1, PS-2, PS-3 and PS-4) with the same depth and diameter at the fully screened wells (Fig 2-1b). Screened intervals of the partial-screened wells are 15 m – 18 m, 21 m – 24 m, and 27 m – 30 m. Water table starts at 14 m from the surface, and the interval length was divided evenly 3 m between 15 m and 30 m interval, evenly. Prior to building CO_2 monitoring network, five full-screened wells were constructed near four partial screened wells. 5 m apart from BS-5, three fully screened wells were constructed and one fully screened well was constructed 7 m apart from BS-8 along groundwater flow direction. The groundwater flow direction of the EIT site is formed from N60W to S60E.The direction of flow was estimated, which was followed by three times of water levels measurements, on July 14th and 30th and October 1st, 2015. The range of measured water levels was between 13.36 m and 16.20 m from the surface. The measured water levels were higher in northwest side than those of southeast side of EIT site. The measured water level lowered toward the side of southeast side and the groundwater flow direction (from N60W to S60E) can be estimated.

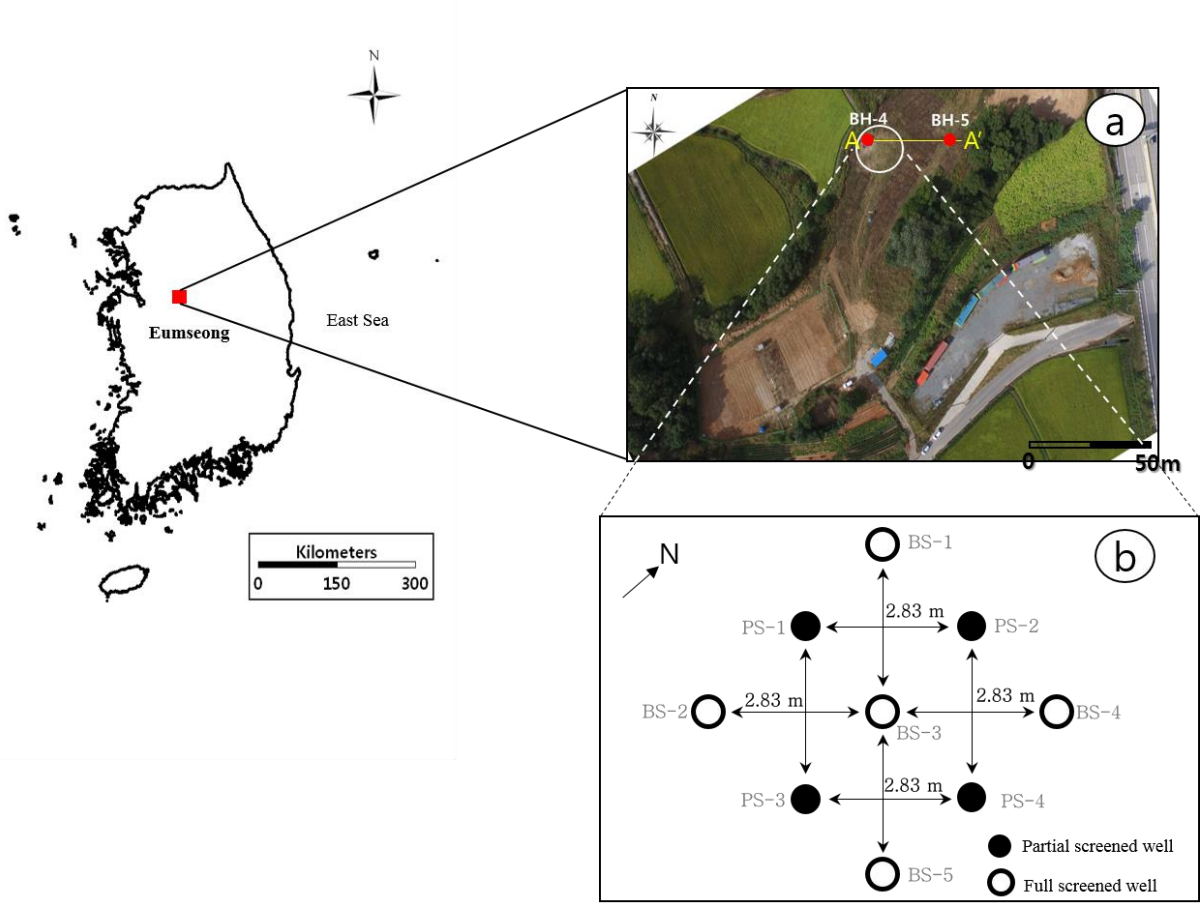

Fig. 2 - 1. Location map (a) EIT site in Eumseong; (b) well arrangement

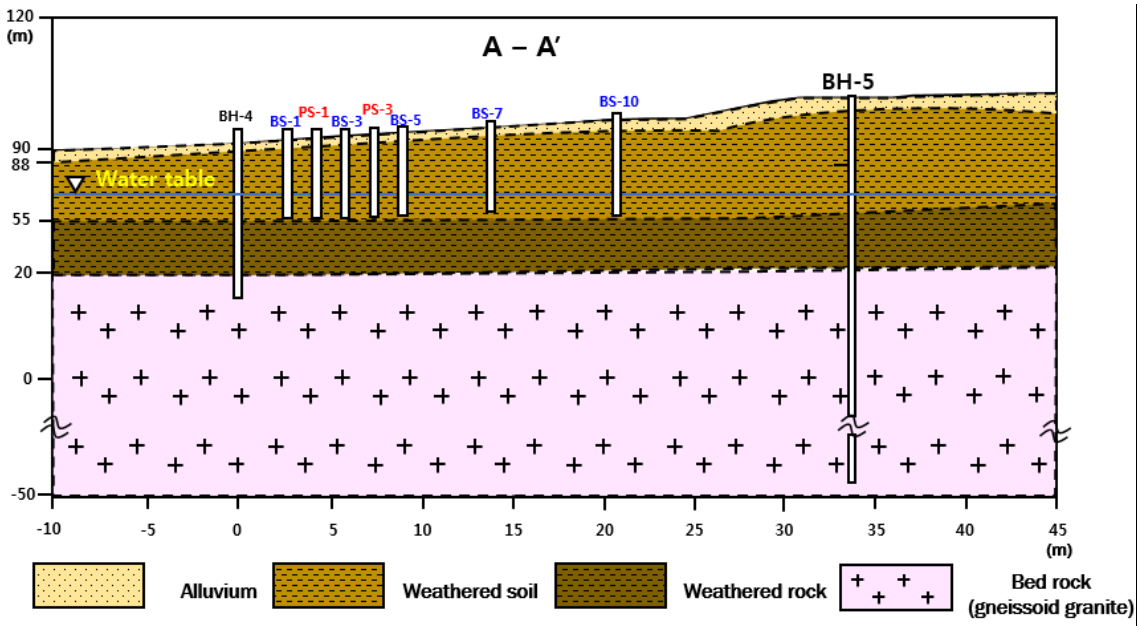

Fig. 2 - 2. Generalized Geologic cross section at EIT site

2.2 Push-Drift-Pull Tracer Tests

A single well push-drift-pull tracer test, referred as an injection and drift-and-pump back test, was studied by Leap and Kaplan (1988) under homogeneous, isotropic, and confined aquifer conditions. They derived the equations to calculate groundwater velocity and effective porosity with taking into account ambient groundwater movement. The movement of tracer plume can be predicted more accurately by using the effective porosity and groundwater velocity

The equation of estimating the groundwater velocity was derived as,

$$V_{LK} = \frac{\sqrt{Qt_{com}/\pi n_e b}}{t_{total}} \quad \text{(Eq. 2-1)}$$

where V_{LK} is the groundwater velocity derived by Leap and Kaplan [m/day]; Q is the extraction rate [m^3/h]; t_{com} is the elapse time from initial pumping until the center of mass of the tracer is arrived to pumping well [h]; n_e is the effective porosity; b is the aquifer thickness [m]; t_{total} is the elapse time from solution injection until the center of mass of the tracer is arrived at pumping well [h].

In this study, the linear velocity and effective porosity were calculated by Hall's method. In Leap and Kaplan's study, they performed push-drift-pull tracer tests in laboratory under homogeneous condition and they could estimate the effective porosity in laboratory. Therefore, in Eq. 2-1, the groundwater velocity can be estimated with the known effective porosity. But, in field test, the effective porosity cannot be estimated. In Hall's study (1991), to overcome this problem, they performed field push-drift-pull tracer tests and derived the equations of groundwater velocity and effective porosity using Darcy's law. The equations are:

$$V_H = \frac{Qt_{com}}{\pi bKit^2_{total}} \quad \text{(Eq. 2-2)}$$

and

$$n_e = \frac{\pi b K^2 i^2 {t_{total}}^2}{Q t_{com}} \quad \text{(Eq. 2-3)}$$

Where V_H is the groundwater velocity derived by Hall [m/day]; K is Hydraulic conductivity [m/sec]; i is the hydraulic gradient [dimensionless].

A push-drift-pull test consists of 3 phases as shown in Fig. 3. The first step is injection phase (so called "push"). In this step, a prepared solution is injected into aquifer at an injection well and the solution is made by mixing a tracer and groundwater together. The second step is drift phase, where the injected solution moves with the ambient groundwater flow. The final step is pumping phase (so called "pull"), where the injected solution is pumped back from the same well. In this study, two partial screened-wells were used as an injecting and extracting well. PS-2 was used in Test 1-1 and PS-1 was used in Test 1-2, Test 2-1 and 1-3. The full screened-wells were used as monitoring wells for push-drift-pull tracer tests.

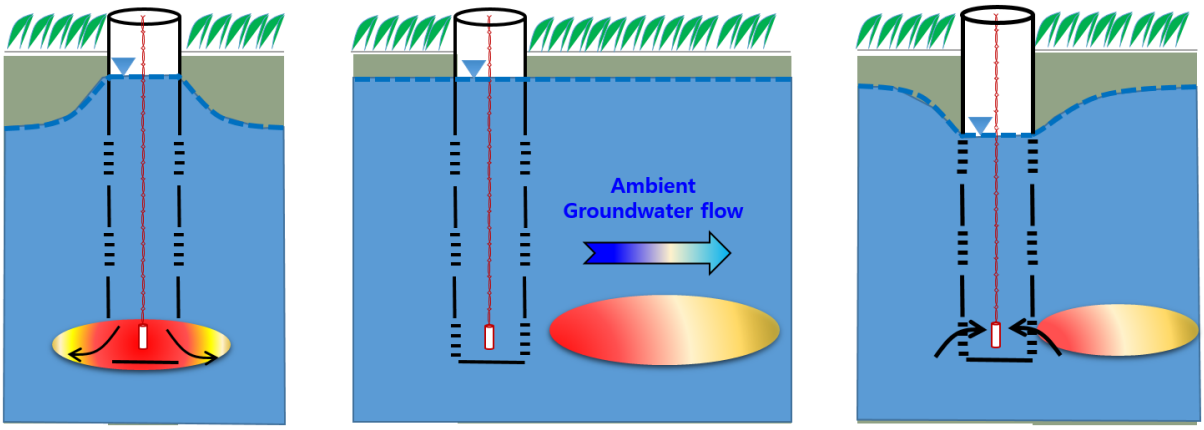

Fig. 2 - 3. Experimental procedures of a push-drift-pull tracer test

Analyzing Method

A conservative tracer in the subsurface transports through pores of the aquifer medium with a dispersion process. It causes decreasing of peak concentration of the tracer but the center of mass of tracer plume moves with average velocity of groundwater (Fig. 2-4). By using this phenomenon, we can calculate the ambient groundwater velocity with push-drift-pull tracer test.

Determination of groundwater velocity from breakthrough curve of single well push-drift-pull tracer test needs t_{com} (the value of time interval from initial pumping to the center of mass of the tracer is pumped in pumping well). The general formula to estimate t_{com} is,

$$t_{com} = \frac{m_1 \cdot t_1 + m_2 \cdot t_2 + \cdots + m_n \cdot t_n}{m_{total}} \quad \text{(Eq. 2-4)}$$

where m_n is the area beneath sampling intervals of tracer breakthrough is curve; t_n is the representative time that is midpoint of the sampling intervals (Fig. 2-5).

When the samples are collected with constant time intervals, t_{com} can be calculated with a minor error (Payne et al., 2008). For this reason, the sampling intervals in this study were set from 2 minutes to 30 minutes until the end of test. The reason of increasing sampling time interval was the efficiency of test. The early time of pull phase, a short time interval for sampling was determined because the peak concentration of tracer is detected generally in the early time of test and the changing of concentration also appears significantly. As progressing the test, interval of sampling time became longer because the low concentration of tracer was expected at the late time of pull phase and the change of concentration would be insignificant.

As obtaining t_{com} derived from Eq. 2-4 and combining it with the hydraulic properties of test condition, we can calculate the groundwater velocity by using Eq. 2-2.

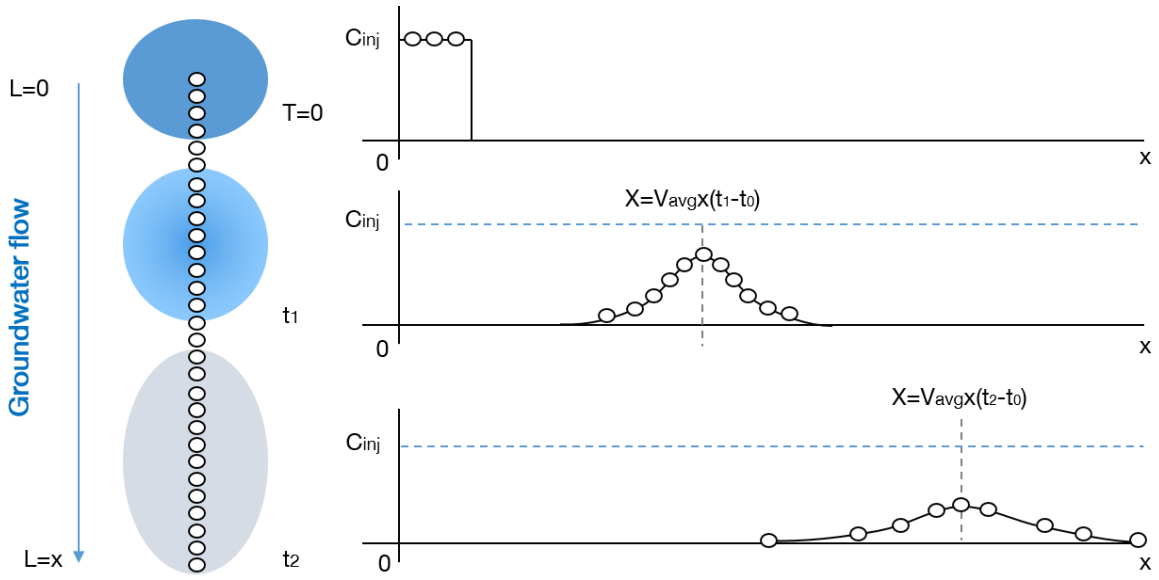

(Modified from Payne et al., 2008)

Fig. 2 - 4. A tracer profile during transportation with dispersion

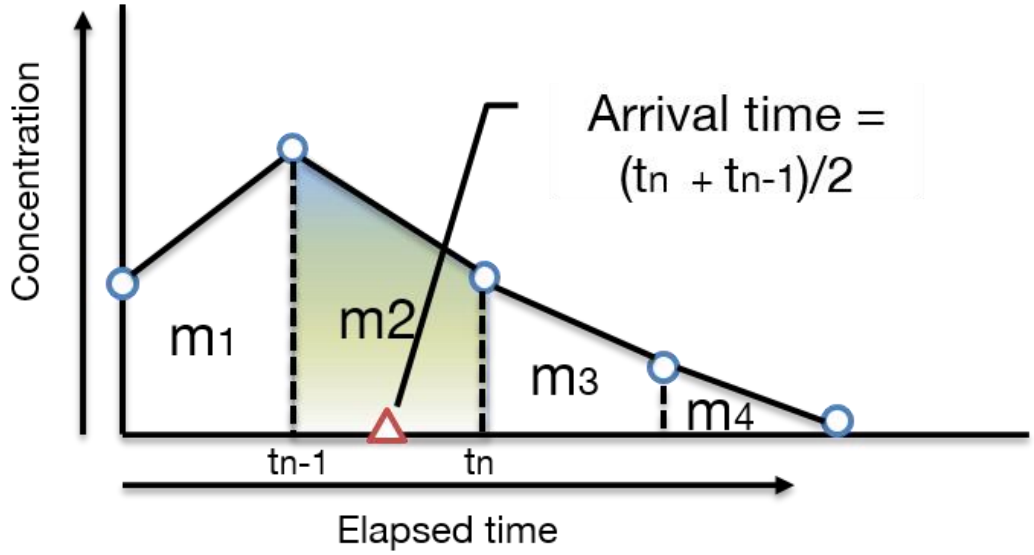

Fig. 2 - 5. Representative time in breakthrough curve between near two sampling points

Field Tests

Total four tests were performed at borehole PS-1 and PS-2. The tested boreholes were partially screened. The hydraulic gradient of EIT site is 0.01 which was calculated by measuring water level in the test well and observation wells near the test well. The hydraulic conductivities of layers were estimated by pumping test at each depth.

In the field tests, multiple tracers (salt and SF_6) were used. The salt tracer was chosen because it is conservative and nonvolatile properties. Also, the SF_6 was used as a conservative and volatile tracer. SF_6 shows similar behaviors as CO_2 because SF_6 is soluble in water and has volatility. However, the reactivity of SF_6 is low and it is usually used as a conservative tracer. The SF_6 was used to investigate the recovery percentage of volatile gas at EIT site as well as the salt tracer which is nonvolatile tracer.

Push Phase

The injection rate was low enough to prevent strong injection flow from disturbing the condition of aquifer. Tracer solution was prepared by mixing 1.2 kg of NaCl (Fig. 7a) and 7 ml of SF_6 (Fig. 7b) into 120 L of ambient groundwater at the study site. After the completion of injection phase, 30 L of chaser (ambient groundwater) was injected to the same injection depth.

During the injection phase, packer (Fig. 7c) was applied in order to isolate the injection interval. By using the packer, the tracer can flow into targeted depth of the aquifer. Calculating the chaser volume was based on the isolated interval and pipe volume (Hebig et al., 2015). Duration of injection was 15 minutes. The injection intervals were 15 - 18m from the surface down to borehole in Test 1-1, 21 – 24 m in Test 1-2 and 2-1, and 27 – 30 m in Test 1-3 (Fig. 6).

Drift and Pull Phase

The drift time was applied about 24 hours in Type 1 (Test 1-1, 1-2 and 1-3) and 50.83 h in Type 2 (Test 2-1). Except the drift time, other test conditions were same as 1-2 in Test 2-1. The extraction rate was 4.46 L/min in Test 1-1, 4 L/min in Test 1-2 and 3.97 L/min in Test 1-3, respectively. The extraction was performed at the isolated intervals by packer. The packer was installed same condition in injection phase. Water was pumped until the concentration of salinity dropped to base-line (background concentration) and durations were 224 minutes in Test 1-1, 425 minutes in Test 1-2, 605 minutes in Test 1-3 and 730 minutes in Test 2-1. The salinity was measured by YSI-556 (Xylem, USA) showed in Fig. 8a and SF_6 was analyzed by using GC-ECD (Koo et al., 2005) showed in Fig. 8b. The water level, temperature, and electrical conductivity were logged in observation bore-holes at the depth to 17 m and 22 m from the surface in Test 1-1 and depth to 22 m and 28 m from the surface in Test 1-2, Test 2-1 and Test 1-3. Total pumped water volumes were 1000 L in Test 1-1, 1700 L in Test 1-2, 2400 L in Test 1-3 and 2050 L in Test 2-1.

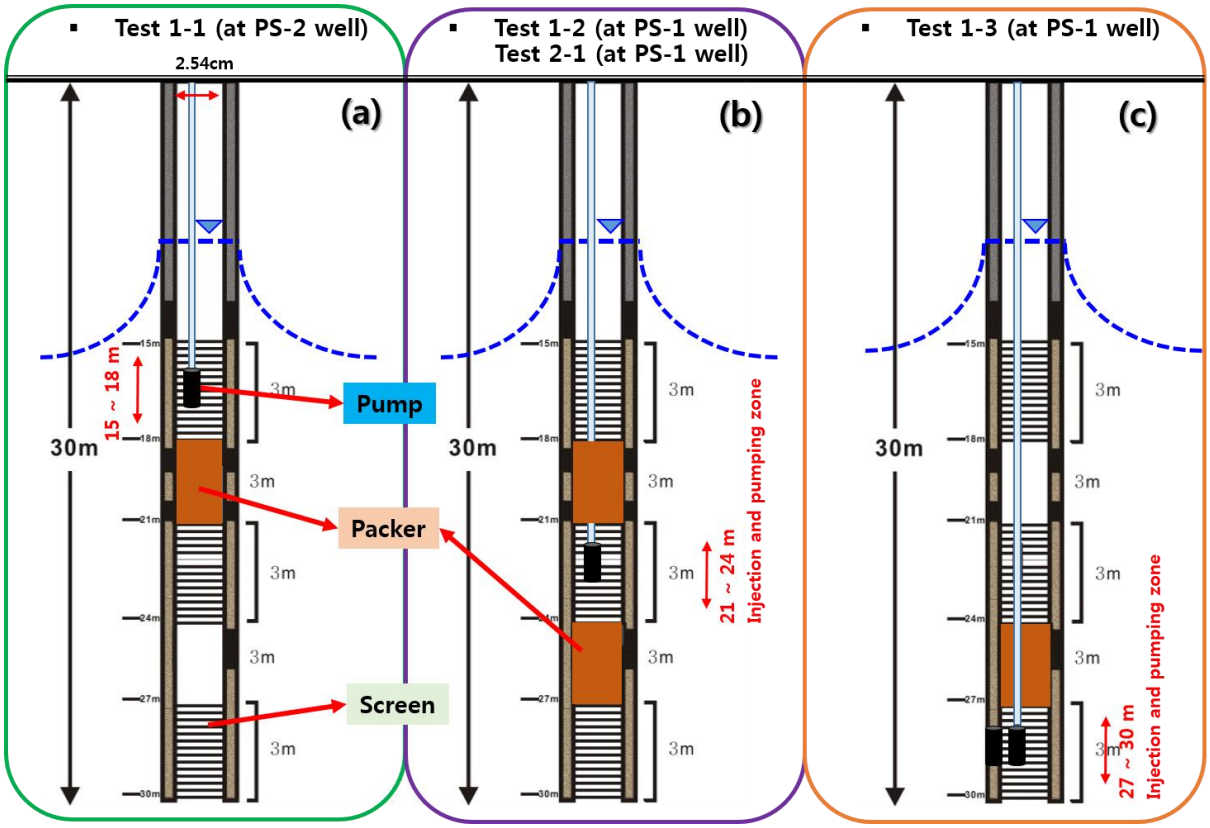

Fig. 2 - 6. Test conditions of field single well push-drift-pull tests

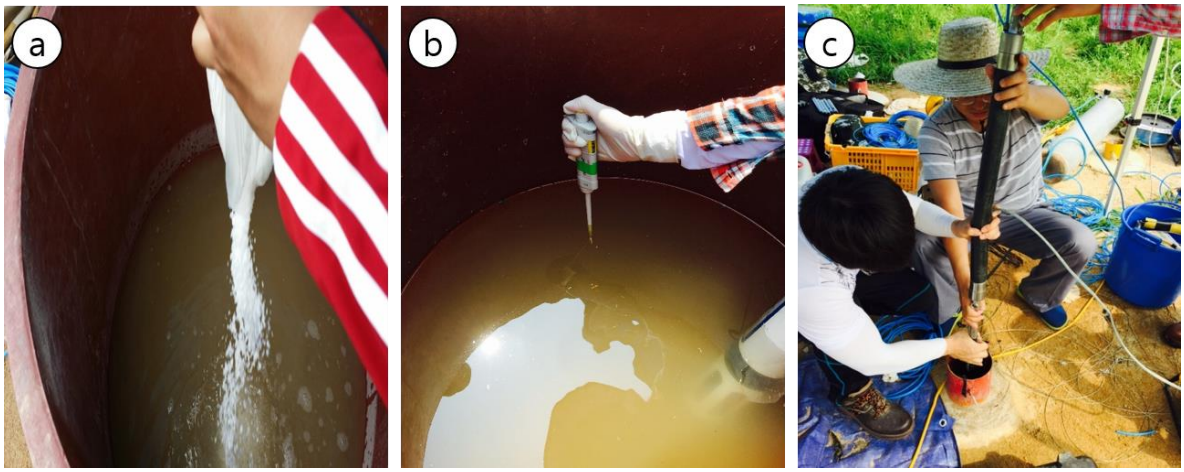

Fig. 2 - 7. Experimental set up during Push phase: (a) sodium chloride, (b) sulfur hexafluoride and (c) packer

Fig. 2 - 8. Devices for measuring concentration of samples: a) YSI-556 to measure the concentration of Salinity and b) GC-ECD to measure SF_6

2.3 Results and Discussions

2.3.1 Push-drift-pull tests at three screened intervals (Type 1)

In type 1, the estimation of hydraulic properties and comparison of recovery percentages were conducted at each screened depth. Three test results (Test 1-1, 1-2, and 1-3) were handled in this section. The breakthrough curves (Fig. 9a, 9b, and 9c) and cumulative mass recovery graphs (Fig. 10a, 10b, and 10c) were illustrated as below. Using the equations (Eq. 2-1 and Eq. 2-2), the groundwater velocity and effective porosity were estimated. The mass recovery percentages of tracers were calculated by trapezoidal method from breakthrough curves. The applied conditions and calculated values were listed in Table 2-1.

The peak concentration of salt was 4.92 ppt (part per thousand) and SF_6 was 822.12 ppt (part per trillion) in Test 1-1. In Test 1-2, the peak concentration value of salt was 1.54 ppt and SF_6 was 4954 ppt. In Test 1-3, the peak concentration value of salt was 2.61 ppt and SF_6 was 2852.31 ppt. The time lasted to show the highest peak concentration was 14 min for salt and 16 min for SF_6 in Test 1-1, 36 min for SF_6 and salt in Test 1-2, and 13 min for salt and 15 min for SF_6 in Test 1-3, respectively. The peak concentrations of both tracers were much lower than the initial concentration of tracers in all tests because of dispersion (Payne et al., 2008). In addition, the time of the highest peak concentration of salt tracer was slightly faster than that of the SF_6 tracer. The breakthrough curves of salt and SF_6 showed different shape. The decreasing gradient of C/C_0 in Test 1-3 was steeper than in Test 1-1 and Test 1-2.

Fluctuation of the SF_6 concentration in Test 1-1, was observed as shown in Fig. 10. Removing the moisture in gasified samples was needed to analyze the SF_6 concentration by GC-ECD. In this process, silica gel was used in Test 1-1 and it was replaced every day to maintain the water removal capability. But, the silica gel has chemical property which absorbs SF_6, so the

fluctuation of SF_6 concentration was occurred on each time after replacing silica gel. Because of absorbing, the mass recovery percentage was not label to calculate in Test 1-1. To avoid absorbing process, Magnesium perchlorate ($Mg(ClO_4)_2$) was used after Test 1-1. As a result, both recovery percentage graph and breakthrough curve can be obtained.

The groundwater velocity was calculated as 0.19 m/d in Test 1-1, 0.21 – 0.35 m/d in Test 1-2, and 0.21 - 0.44 m/d in Test 1-3, while the mass recovery percentage of salt tracer was 97 % in Test 1-1, 97 % in Test 1-2, and 90 % in Test 1-3. But the mass recovery percentage of SF_6 in Test 1-2 and Test 1-3 were only 23 % and 62 %, respectively. Most of the salt tracer was recovered but the extracted mass of the SF_6 tracer was less than half of the injected mass. The difference of mass recovery percentage between salt and SF_6 is expected due to volatility of the SF_6 tracer (Addy et al., 2002). The mass recovery rate of tracers is the fastest in Test 1-1 and the recovery rate become slow as increasing the test depth. It can be explained that the interval between 27 – 30 m has low permeability zone because of long tailing and slow mass recovery rate. Lessoff and Konikow (1997) showed that when a tracer moves away from the well in a channel of high permeability, while drifting into a lower permeability zone. Then, tracer is pulled back to the well through the low permeability zone, while leaving a trace of significant tailing in the recovery curve.

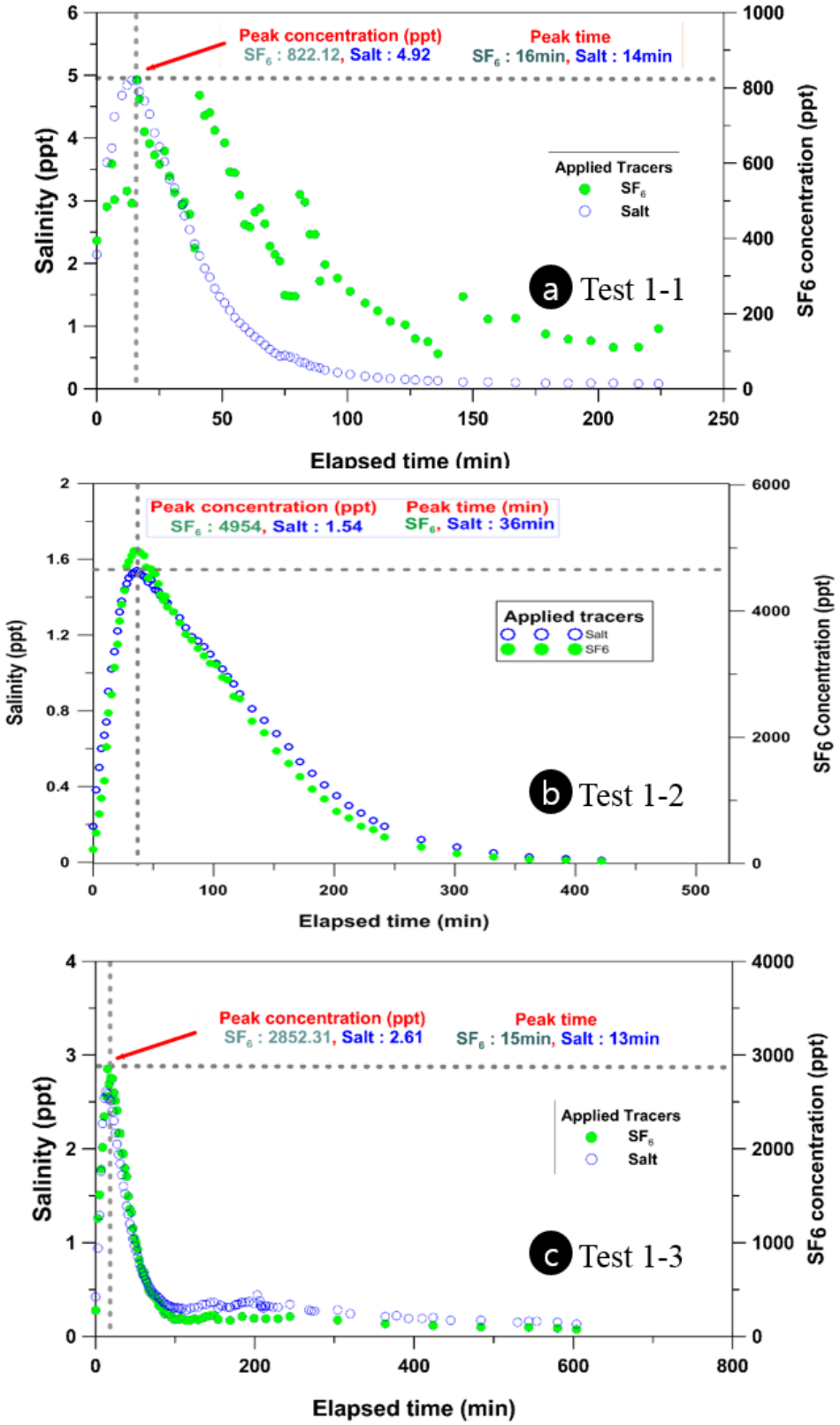

Fig. 2 - 9. Tracer (Salt and SF_6) breakthrough curves in (a) Test 1–1 (15 – 18 m), (b) Test 1-2 (21 – 24 m) and (c) Test 1-3 (27 – 30 m)

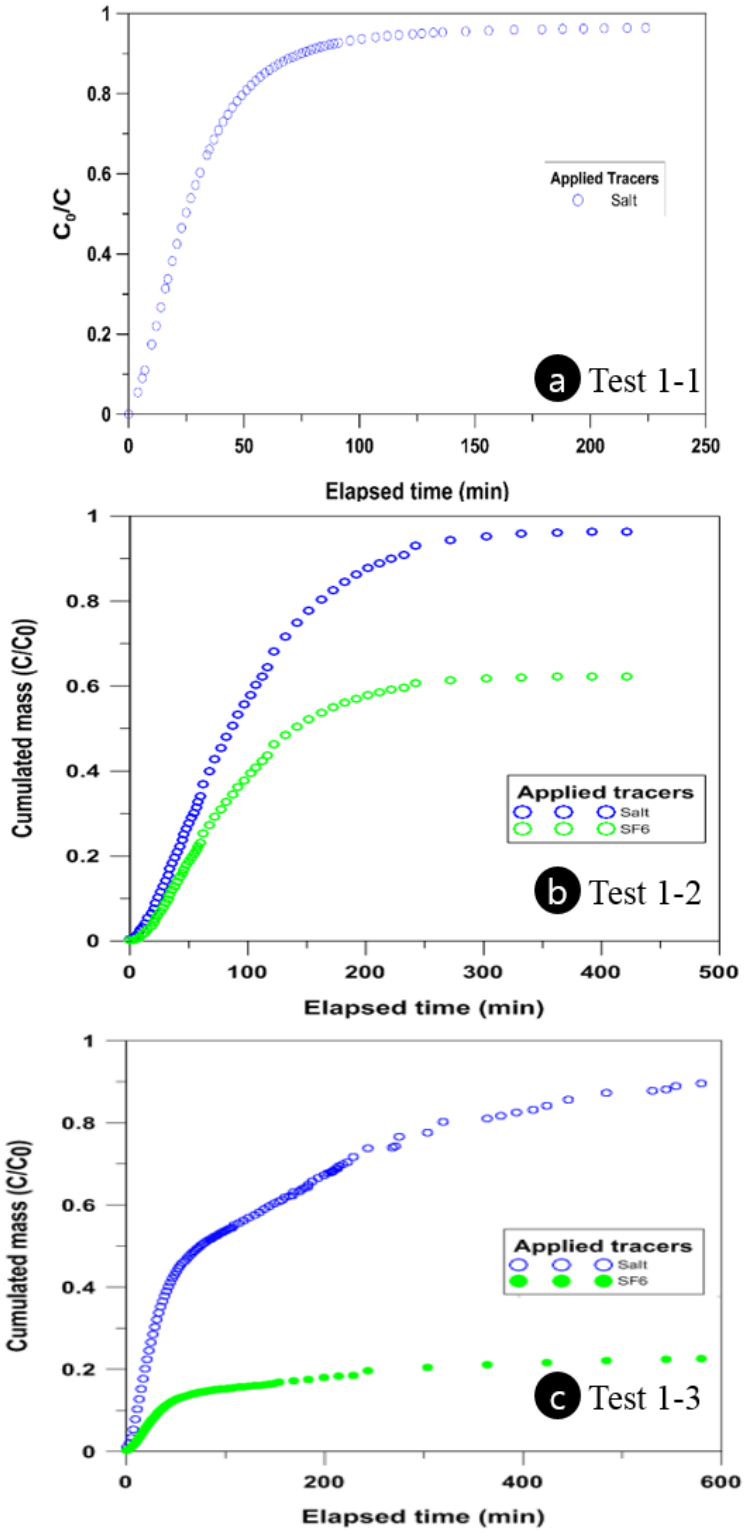

Fig. 2 - 10. Cumulative mass recovery percentage graphs in (a) Test 1–1 (15 – 18 m), (b) Test 1-2 (21 – 24 m) and (c) Test 1-3 (27 – 30 m)

2.3.2 Push-drift-pull tests under different drift times (Type 2)

In order to investigate the influence of drift time when a push-drift-pull tracer test was performed, all other conditions were remained the same except the drift time. 24-hour of drift time was applied at the previous push-drift-pull test (Test 1-2), on the other hand, longer drift time of 51-hour was applied to the next test (Test 2-1). All the detail information was listed on the table 2-1.

The results are shown in Fig. 11. The most noticeable difference was lower concentration of SF_6 than Test 1-2. The peak concentration of SF_6 was 4,954 ppt in Test 1-2, and 1,046 ppt in Test 2-1. In contrast with, the peak concentration of salt was nearly same in both tests. It indicates that SF_6 tracer was volatilized with longer drift time. The total elapsed time until the end of test in Test 2-1 was about 300 minutes longer than Test 1-2, and it was caused by the longer drift time. Based on the results of Test 2-1, linear velocity and recovery percentage were calculated. As a result, the estimated linear velocity was 0.1 m/d and recovery percentage was 26 % (Fig. 12). Also, the arrival time of peak concentration was same in Test 2-1. However, in Test 2-2, the arrival time of SF_6 was 43 minutes more delayed than salt tracer. In case of Type 1, the arrival time of salt was slightly faster than SF_6. In Test 2-1, the difference of arrival time between two types of tracers was about 43 minutes. As increasing drift time, the gap of arrival time was increased. Lower linear velocity was derived in longer drift time condition, and it shows consistently with study of Hwang (2002). The author figured out the underestimation of linear velocity is caused by increasing drift time. Also, the recovery percentage of SF_6 was lower than type 1. On the other hand, the recovery percentage of salt was same because of its non-volatility property. From this result, unrecovered SF_6 tracers might be volatilized during longer drift time.

To avoid biased test results from a push-drift-pull tracer test with volatile tracer, it is important

to set a proper length of drift time. Excessive long drift time setting for volatile tracer during drift phase can cause difficult detection of tracer at study site.

2.3.3 Building the effective monitoring network at EIT site

By using the estimated groundwater velocity from the push-drift-pull test, the position of additional monitoring wells can be decided by predicting the movement of injected CO_2 plume flowing through ambient groundwater. Also, additional to previous well arrangement (Fig. 13), monitoring wells were constructed to detect volatilized CO_2 in unsaturated zone. Loss of volatile tracer was investigated during fate of transport to make a comparison between non-volatile and volatile tracers in this study. The CO_2 also has volatility and it can be volatilized from subsurface during fate of transport. For this reason, the monitoring wells in unsaturated zone should be constructed. Based on the results of push-drift-pull tests, the effective monitoring network can be built at EIT site (Fig. 14 and Fig. 15).

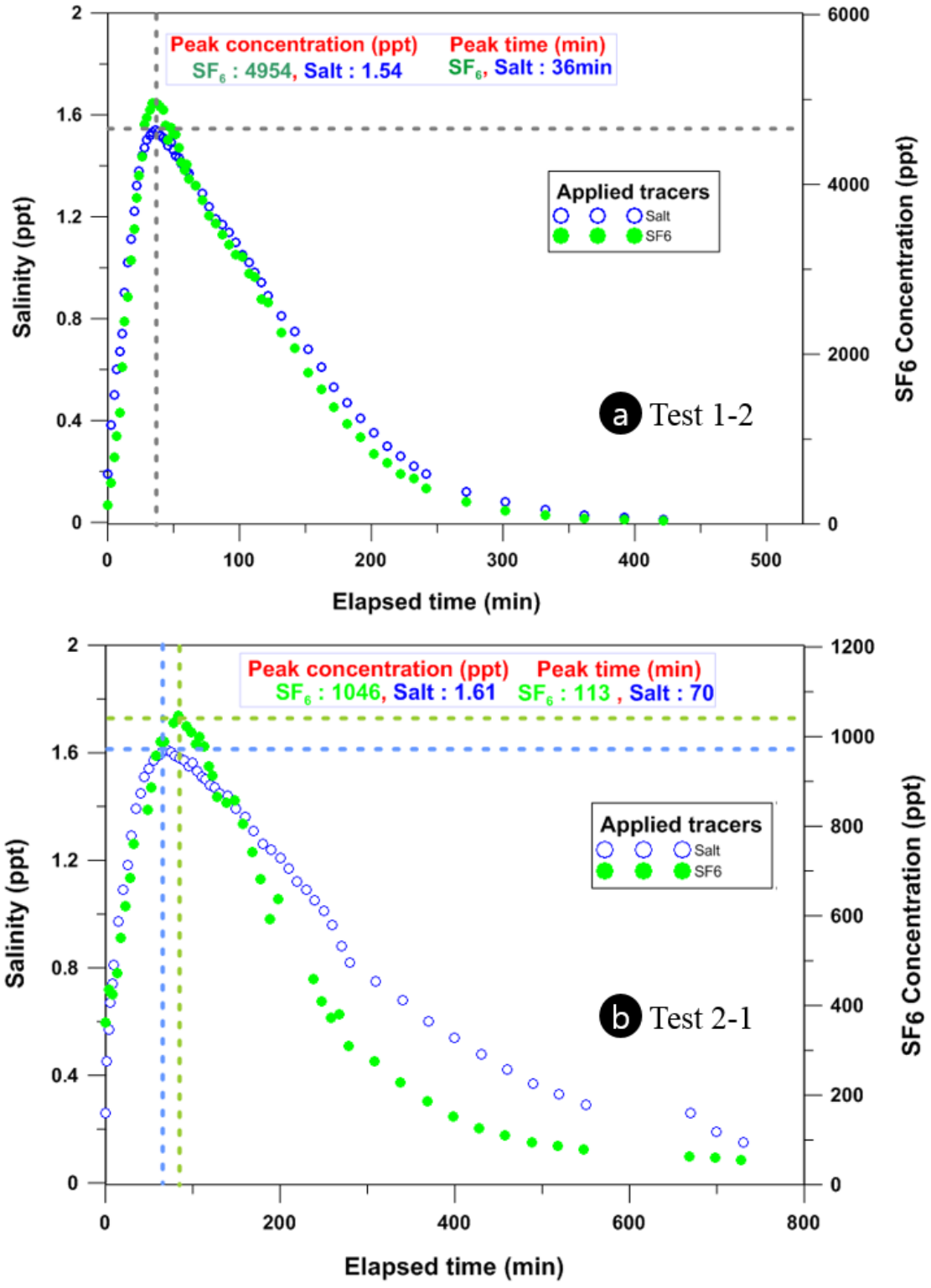

Fig. 2 - 11. Tracer (Salt and SF_6) breakthrough curves in (a) Test 1–2 (21 – 24 m), (b) Test 2-1 (21 – 24 m)

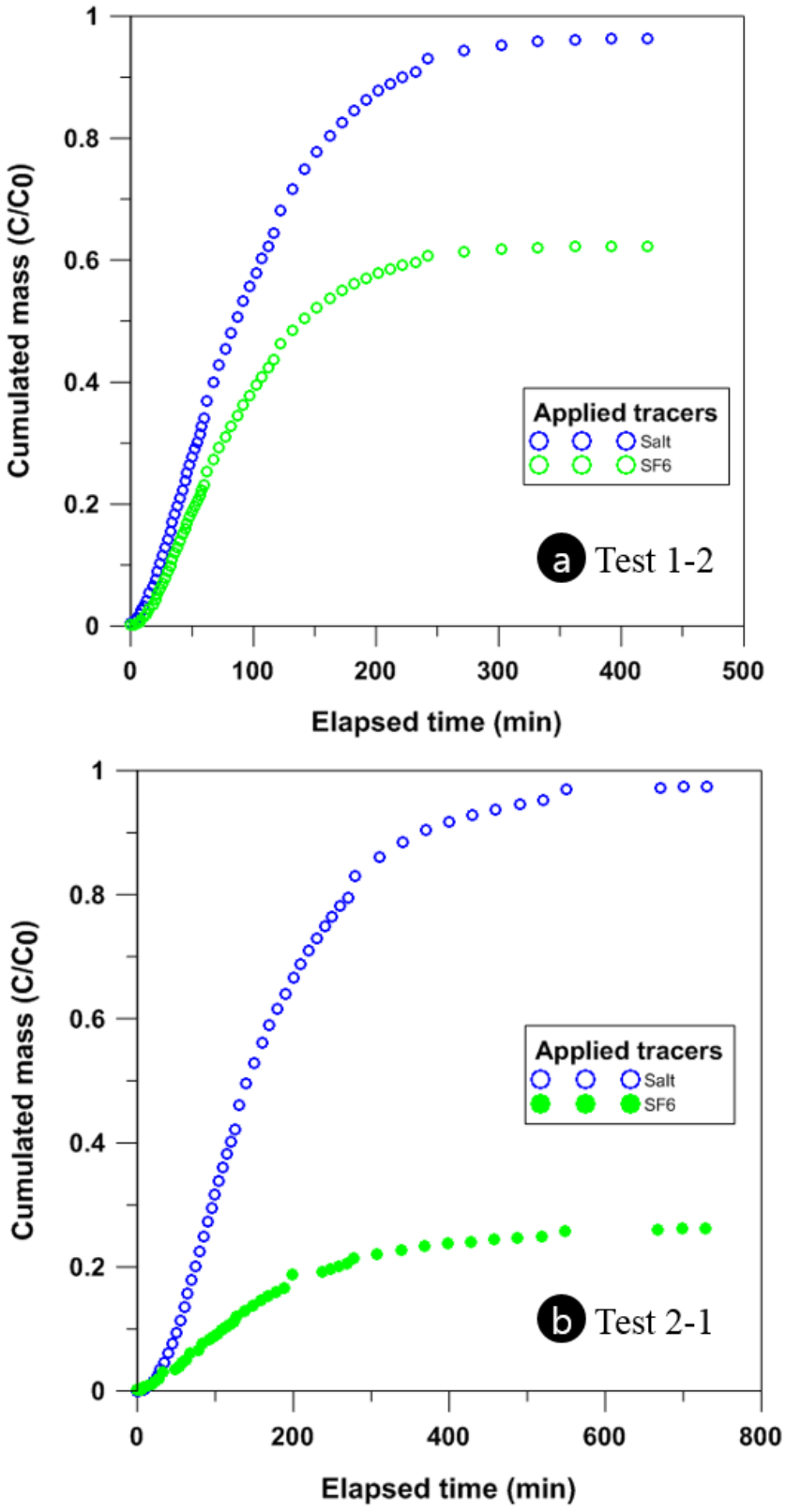

Fig. 2 - 12. Cumulative mass recovery percentage graphs in (a) Test 1–2 (21 – 24 m), (b) Test 2-1 (21 – 24 m)

Table 2 - 1 Calculated linear velocity and effective porosity by push-drift-pull tracer tests

	Hydraulic properties		Tracer	Linear velocity (m/d)	Effective porosity
Test 1-1	Pumping rate (m^3/h)	0.27	Salt	0.19	0.03
	Aquifer thickness (m)	47			
	Drift time (h)	24.13			
	Center of mass time (h)	0.52			
	Hydraulic conductivity (m/sec)	5.6×10^{-6}			
	Hydraulic gradient	0.01			
Test 1–2	Pumping rate (m^3/h)	0.24	Salt	0.35	0.02
	Aquifer thickness (m)	47			
	Drift time (h)	24			
	Center of mass time - Salt (h)	1.73			
	Center of mass time – SF_6 (h)	1.64	SF_6	0.21	0.07
	Hydraulic conductivity (m/sec)	8.1×10^{-6}			
	Hydraulic gradient	0.01			

Test 1–3	Pumping rate (m^3/h)	0.24			
	Aquifer thickness (m)	47	Salt	0.44	0.02
	Drift time (h)	24.47			
	Center of mass time - Salt (h)	2.54			
	Center of mass time – SF_6 (h)	2.30	SF_6	0.21	0.07
	Hydraulic conductivity (m/sec)	8.6×10^{-6}			
	Hydraulic gradient	0.01			
Test 2–1	Pumping rate (m^3/h)	0.17			
	Aquifer thickness (m)	47	Salt	0.10	0.07
	Drift time (h)	50.83			
	Center of mass time - Salt (h)	3.19			
	Center of mass time – SF_6 (h)	3.23	SF_6	0.10	0.07
	Hydraulic conductivity (m/sec)	8.1×10^{-6}			
	Hydraulic gradient	0.01			

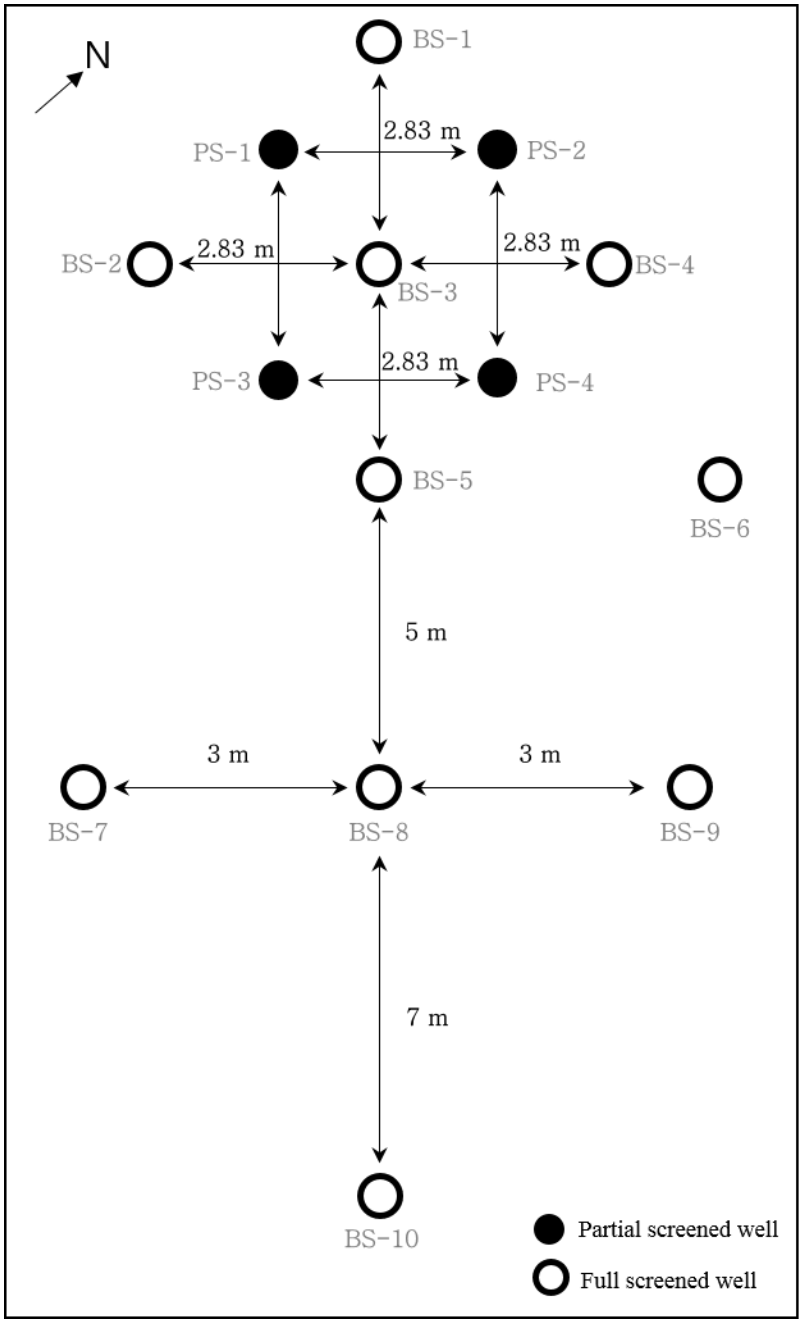

Fig. 2 - 13. Previous well arrangement at EIT site before constructing additional monitoring wells

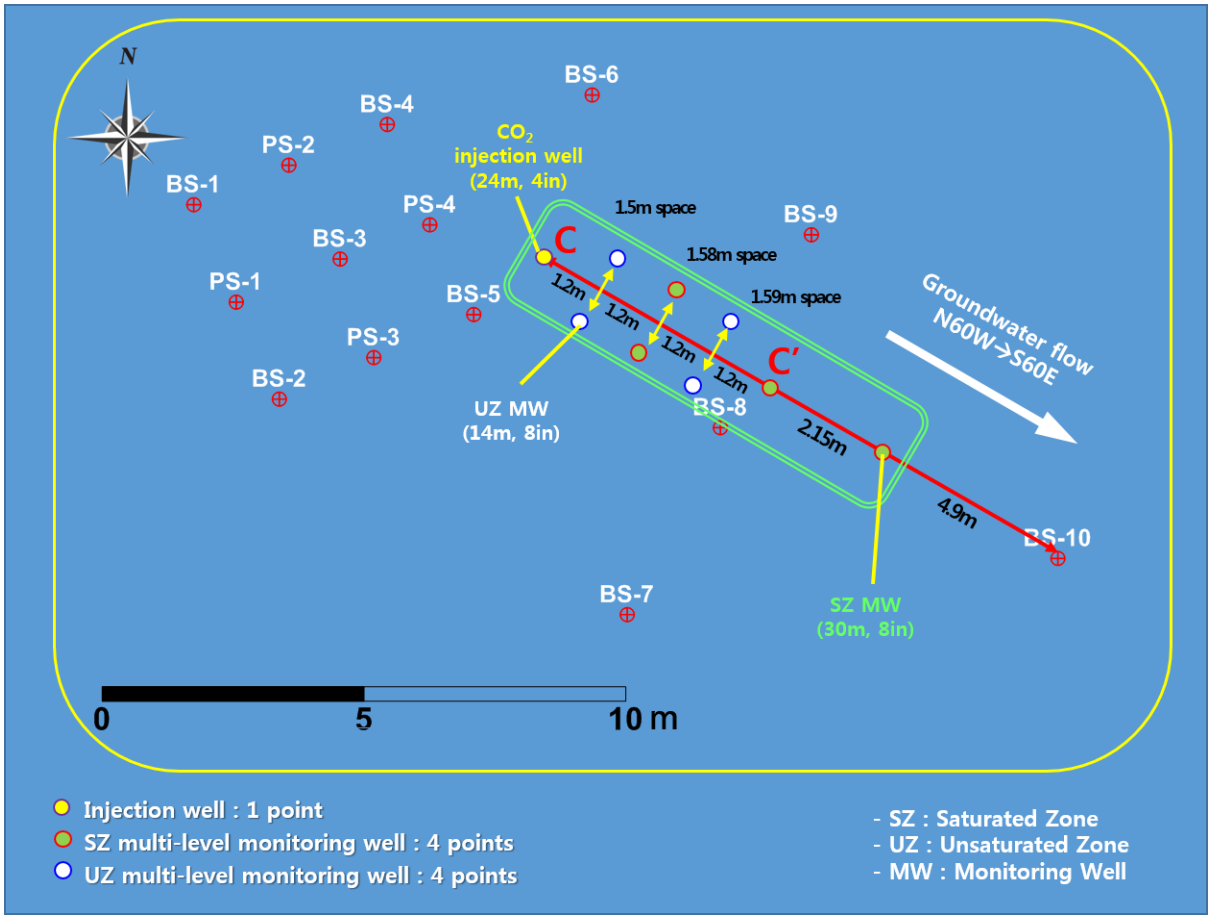

Fig. 2 - 14. Monitoring network with additional constructed wells (green box) after push-drift-pull tracer tests

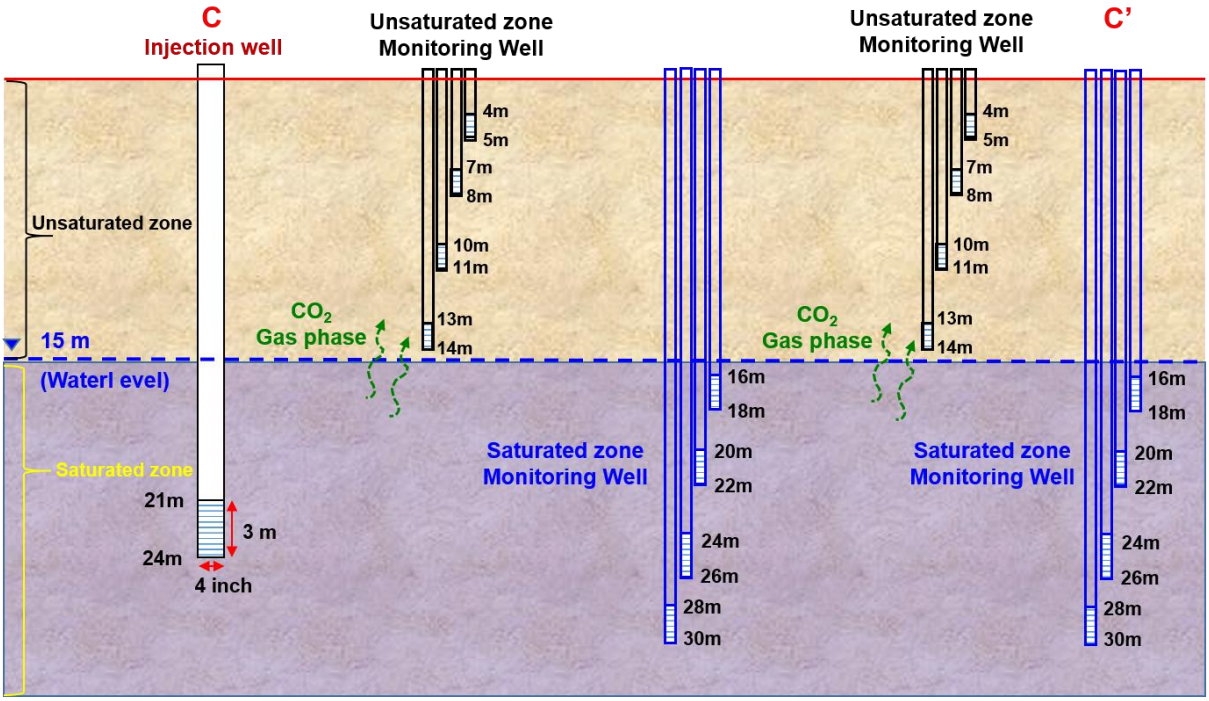

Fig. 2 - 15. Schematic of cross section C-C' (in green box) with additional constructed wells after push-drift-pull tracer tests

3 LABORATORY EXPERIMENT

3.1 Methods and Materials

3.1.1 Experimental Setup and Deign

The sand tank was made to investigate the process of solute transport in various hydraulic conditions with bromide. Potassium bromide was used as a conservative tracer.

The tank was made of acryl glass with inner dimensions of 120 cm × 50 cm × 60 cm (length × width × height) as shown in Fig. 3-4a. The thickness of acryl glass is 2 cm. The hydraulic gradient of tests was maintained by two constant head chambers (10 cm × 50 cm × 60 cm) that were positioned at both sides of tank. As controlling the water level of both chambers, the various hydraulic gradients can be generated. The partitioning plates consist of two plates (Fig. 3-4c) to fix the fine mesh. The fine mesh was inserted between partitioning plates to prevent sand grains passing through water chamber from sand tank.

For injecting and extracting water, the test wells were made of 2 mm thick acrylic pipe with the inner diameter of 2 cm (Fig. 3-5). The length of slots was decided as the same ratio of field wells. The length of slotted interval is 5 mm and the ratio of slotted interval to full length of acrylic pipe is one-tenth.

Experimental Design

Push-drift-pull experiments were conducted under various conditions, which were drift times, input concentrations, hydraulic gradients, and penetrating depths.

The first variable condition was drift time. Hwang (2004) already performed push-drift-pull tests with the variable drift time and found out the effects of the drift time. In this study, it was performed under different hydraulic gradient condition with several different drift

times of 3, 5, 8 and 10 minutes.

The second variable condition was input concentration of KBr to investigate the effect of density in push-drift-pull tracer tests. The applied concentration values of tracer were from 174 mg/L to 2450 mg/L. They were measured by bromide selective electrode. According to Barth's study (2001), 238 mg/L of KBr didn't cause density induced sinking. But over the 238 mg/L, the tracer solution can be influenced by density induced sinking. By comparing the results, the effect of density can be figured out.

The third variable condition was hydraulic gradient. The hydraulic gradients were controlled by water chambers. The applied hydraulic gradients were 3×10^{-3}, 8×10^{-3} and 1.2×10^{-2}.

The fourth variable condition was penetrating depth. Three acryl wells were arranged in a sand tank with different penetrating depths. The wells were positioned from bottom to 20 cm above from the bottom with 10 cm intervals.

During push-drift-pull tests, the hydraulic conductivity of sand was 15 cm/min. A constant injection/extraction rate was applied considering the background flow velocity in all tests as 6 ml/min and 10 ml/min, respectively.

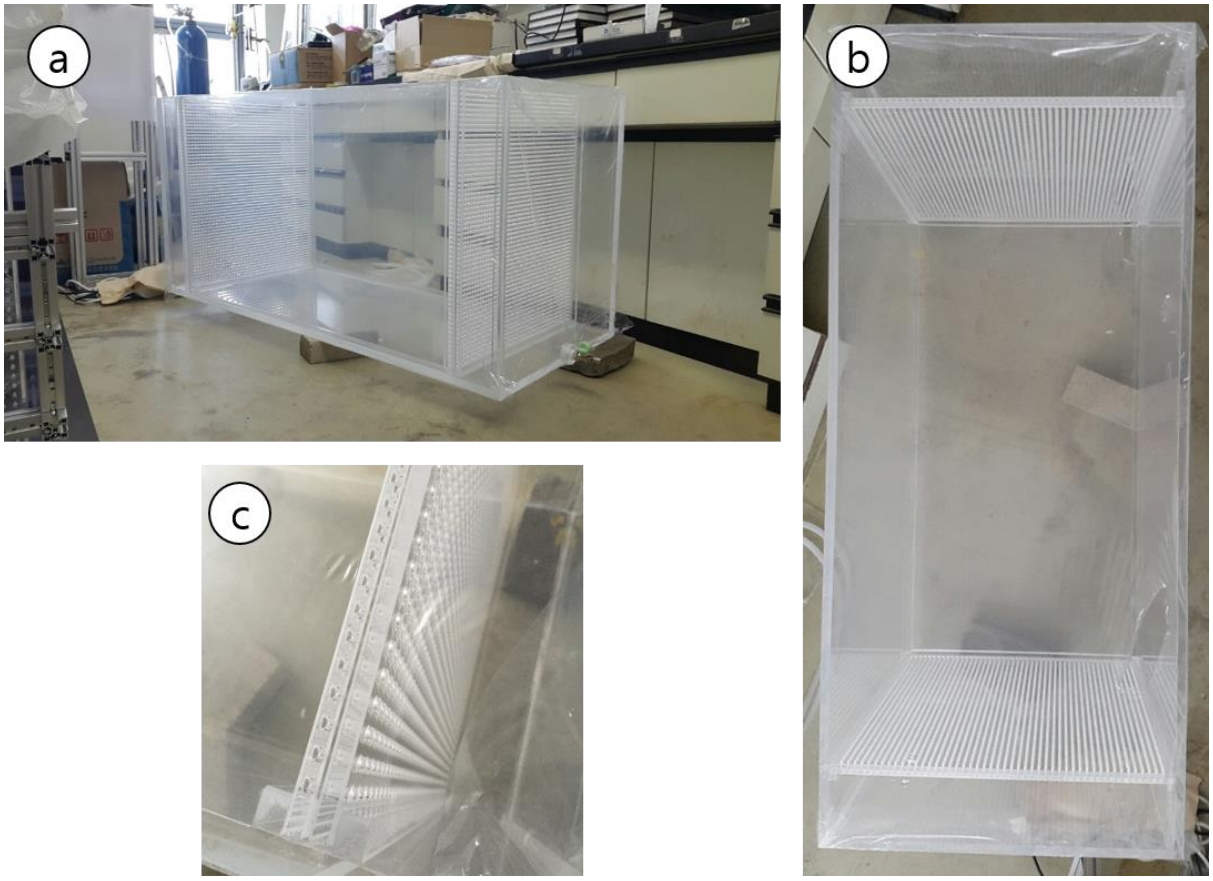

Fig. 3 - 1. An acrylic sand tank (120 cm x 50 cm x 60 cm) to transport solution through filled sand (a,b) and slot to insert fine mesh (c)

Fig. 3 - 2. An acrylic pipe of ø 20 mm (i.d.) and 0.7 m length with 5 mm slot intervals

3.1.2 Measurement of hydraulic parameters

The Joomoonjin silica sand was used to fill in the middle part of chamber. A set of sieves was performed to identify the middle particle diameter (d_{50}) and the uniformity of the materials. The d_{50} of sand was 1.28 mm.

The hydraulic conductivity was measured by performing constant permeability tests. The length of column was 170 mm and head difference values were 7.3 cm, 5.6 cm and 3.6 cm, respectively. Total nine tests were repeatedly performed for each size of sand and the average value was chosen as a representative value. The averaged hydraulic conductivity is given in Table 3-1.

To estimate the effective porosity of sand materials, column tests were performed. The acrylic column length was 210 mm and was filled with sand materials. A 5TE sensor (DECAGON, USA) was used to measure the soil moisture content and the sensor and located in the sand column to measure the volumetric content of porous medium. The water content was measured for 5 days after gravity drainage and the value was 0.02 (Fig. 3-6). The value can be considered as a field capacity because the drainage was fully completed. The effective porosity is defined as total porosity minus field capacity and the estimated relative effective porosity of sand is shown in Table 3-1.

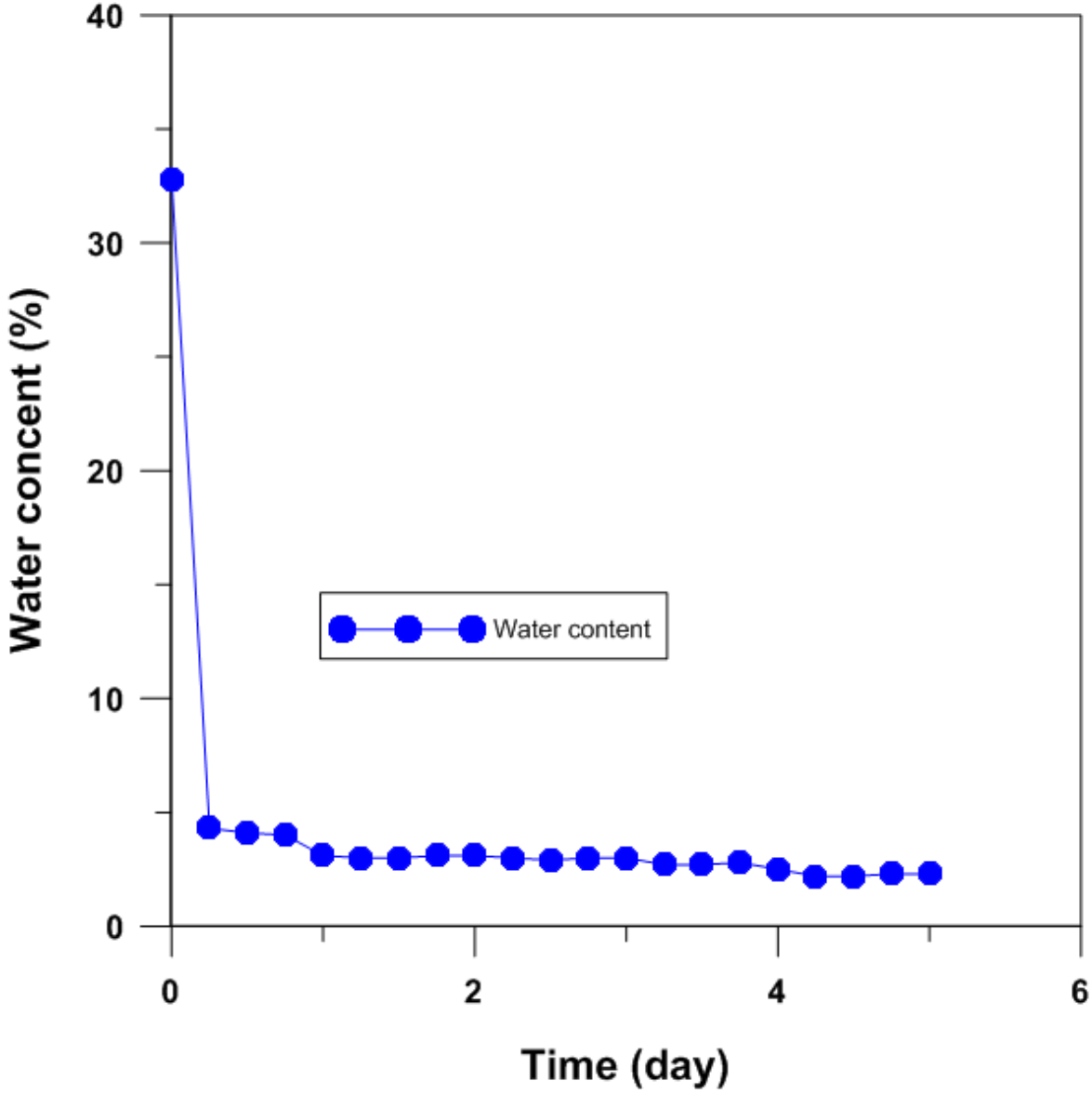

Fig. 3 - 3. Water content (%) measured for 5 days by 5TE sensor

Table 3 - 1 Measured hydraulic properties of sand

Parameter	Test sand
Particle size (mm)	1.28
Bulk density (g/cm^3)	1.65
Effective porosity	0.32
Field capacity	0.02
Hydraulic conductivity (cm/min)	15 ± 0.93

3.1.3 Establishment of Measurement Device

The Br^- ion selective electrode (HORIBA, JPN) was used to measure the real time concentration of bromide during push-drift-pull tracer tests (Fig. 3-7a). The measuring range of bromide electrode is from 0.8 ppm to 80,000 ppm as it can measure the ion concentration with reference electrode. Several simple tests were performed to test the accuracy of ion concentration measured by ion selective electrode. The number of calibration points was three. The standard Potassium Bromide (KBr) solution was prepared by mixing solid KBr (Fig. 3-7b) and deionized water with a stirrer (Fig. 3-7c). To enhance the accuracy of measured concentration, the concentration of standard solutions need to cover the range of real tests. For example, if the concentration range of real test from 50 mg/L to 1500 mg/L, the calibration concentration is from under 50 mg/L to over 1500 mg/L. The used deionized water volume was 200 mL and the concentration of standard solutions was 40mg/L, 859 mg/L and 1679 mg/L respectively. After calibration, five samples of bromide solution were measured by ion selective electrode and compared the measured concentration with calculated concentration values. Fig. 3-8 shows the result of performance test. The X-axis is calculated concentration and Y-axis is measured concentration. The calibration tests were performed for three times and the test results were similar to each other, with 0.99 R-squared value. In laboratory-scale push-drift-pull tests, the calibration test was performed prior to starting experiments for the reliable measurement.

Fig. 3 - 4. Materials for calibration and performance test: a) Bromide ion selective electrode, b) solid KBr and c) stirrer to make solution

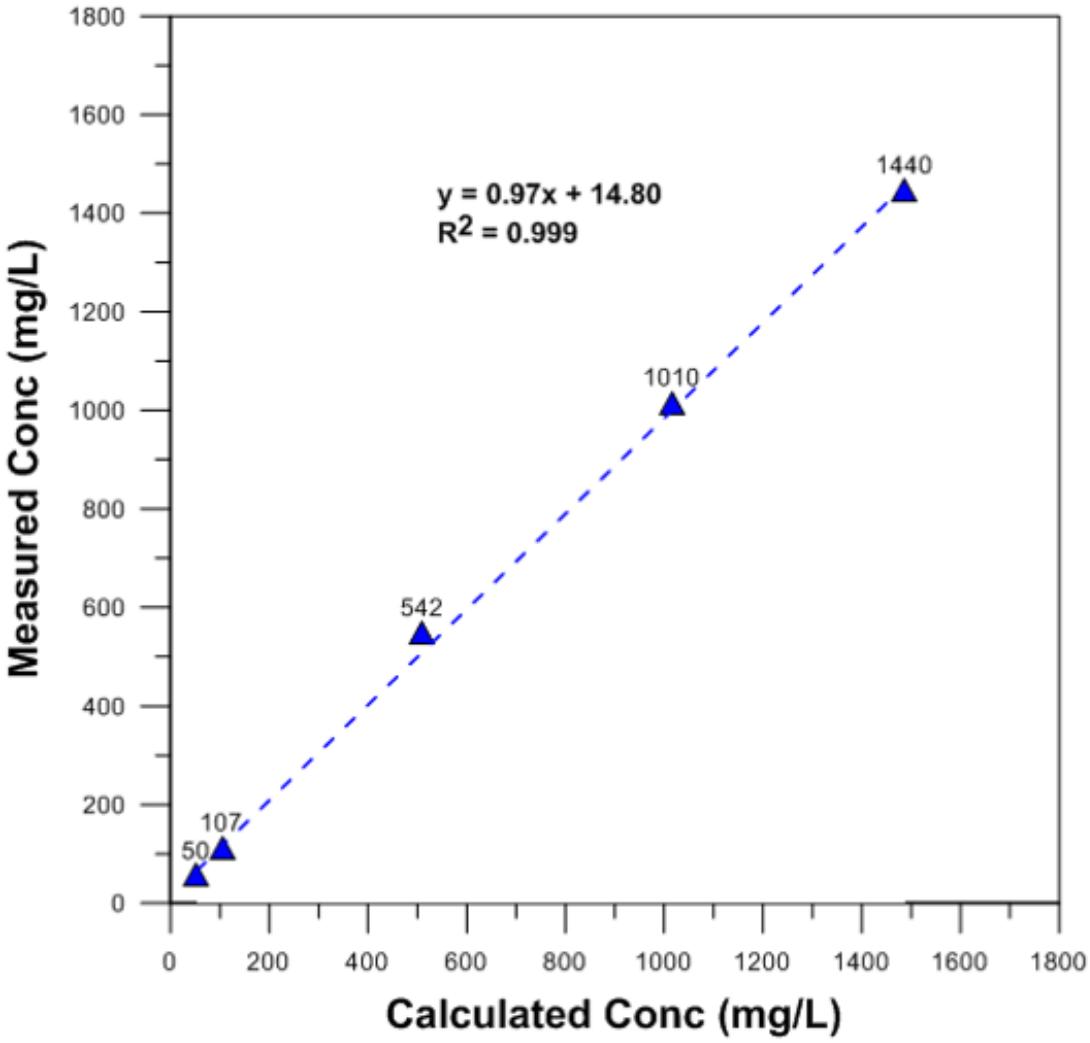

Fig. 3 - 5. Result of ion selective electrode. 3 points calibration was done and total 4 random concentration samples were measured by the electrode

3.1.4 Numerical approach

Numerical models were constructed to reproduce an analogous system with the experimental push-pull tracer test. With the numerical models, reasons for the bias of the estimated groundwater velocities between the experimental settings and tracer tests would be interpreted. Also, to overcome the density driven effects of the injected tracer with different hydraulic flow fields, an adequate extracting rate for the push-pull test would be suggested from the modeling work. The HydroGeoSphere modeling program (Therrien et al., 2010), which can simulate the groundwater flow and the variably-density solute transport, was used in this study.

Governing equations

The following equations denote variable-density flow and solute transport in 3D porous media:

$$-\frac{\partial q_i}{\partial x_i} = S_s \frac{\partial h_0}{\partial t} \qquad \text{i = 1, 2, 3} \qquad \text{(Eq. 3-1)}$$

$$\frac{\partial}{\partial x_i}(\emptyset D_{ij} \frac{\partial c}{\partial x_j} - q_i C) = \frac{\partial(\emptyset C)}{\partial t} \qquad \text{i,j = 1, 2, 3} \qquad \text{(Eq. 3-2)}$$

where

q_i $[LT^{-1}]$ Darcy flux

S_s $[L^{-1}]$ Specific storage

h_0 $[L]$ equivalent freshwater head

$\emptyset$ $[-]$ matrix porosity

D_{ij} $[L^2T^{-1}]$ hydrodynamic dispersion

c $[-]$ solute concentration, expressed as relative concentration

The specific storage S_s is defined as:

$$S_s = \rho_0 g(\alpha + \emptyset\beta) \qquad \text{(Eq. 3-3)}$$

where

ρ_0 $[ML^{-3}]$ freshwater density

g $[LT^{-2}]$ gravitational acceleration

α $[M^{-1}LT^2]$ matrix compressibility

β $[M^{-1}LT^2]$ fluid compressibility

The variable-density Darcy flux, q_i, is a function of freshwater head, h_0, and solute concentration, c. Darcy fluxes for matrix and fracture are given by:

$$q_i = -K_{ij}(\frac{h_0}{\partial x_j} + \gamma c \eta_j) \qquad \text{i,j = 1, 2, 3} \qquad \text{(Eq. 3-4)}$$

where

K_{ij} $[LT^{-1}]$ freshwater hydraulic conductivity of matrix

η_j $[-]$ flow direction coefficient: 0 is horizontal direction; 1 is vertical direction

γ [–] maximum relative density, $\gamma = \left(\frac{\rho_{max} - \rho_0}{\rho_0}\right) - 1$

ρ_0 $[ML^{-3}]$ freshwater density

ρ_{max} $[ML^{-3}]$ maximum fluid density

Model Setup

According to the settings of the sand tank experiment, a three-dimensional model domain was generated as shown in Fig. 4. The variably-sized grids were created while finer grids were inserted near the tested well and coarser grids when of distance from the well point increases. The generated numbers of node and element were 8721 and 7488, respectively. The left side and right side nodes of model (x = 0 m and x = 1 m) are assigned as Dirichlet flow boundary conditions to create the constant hydraulic gradient. Other boundaries are no-flow boundary. The well node for injection and extraction was generated at the same point of laboratory experiment, and the initial concentration of all nodes were $C_0 = 0$. Model parameters for the numerical simulation are shown in Table 2. The hydraulic properties were estimated by laboratory test and the free-solution diffusion coefficient of KBr was applied $2.02 \times 10^{-9}\ m^2/s$ (Shackelford and Daniel, 1991).

Modeling calibration was implemented as generating the same tracer test conditions with the laboratory experiments. Through trial and error approaches, model parameters of dispersivity was adjusted to lower the differences in the breakthrough curves between the experiments and simulations. After the model calibration, changes in the variables which affect the results of the push-pull tracer test were implemented.

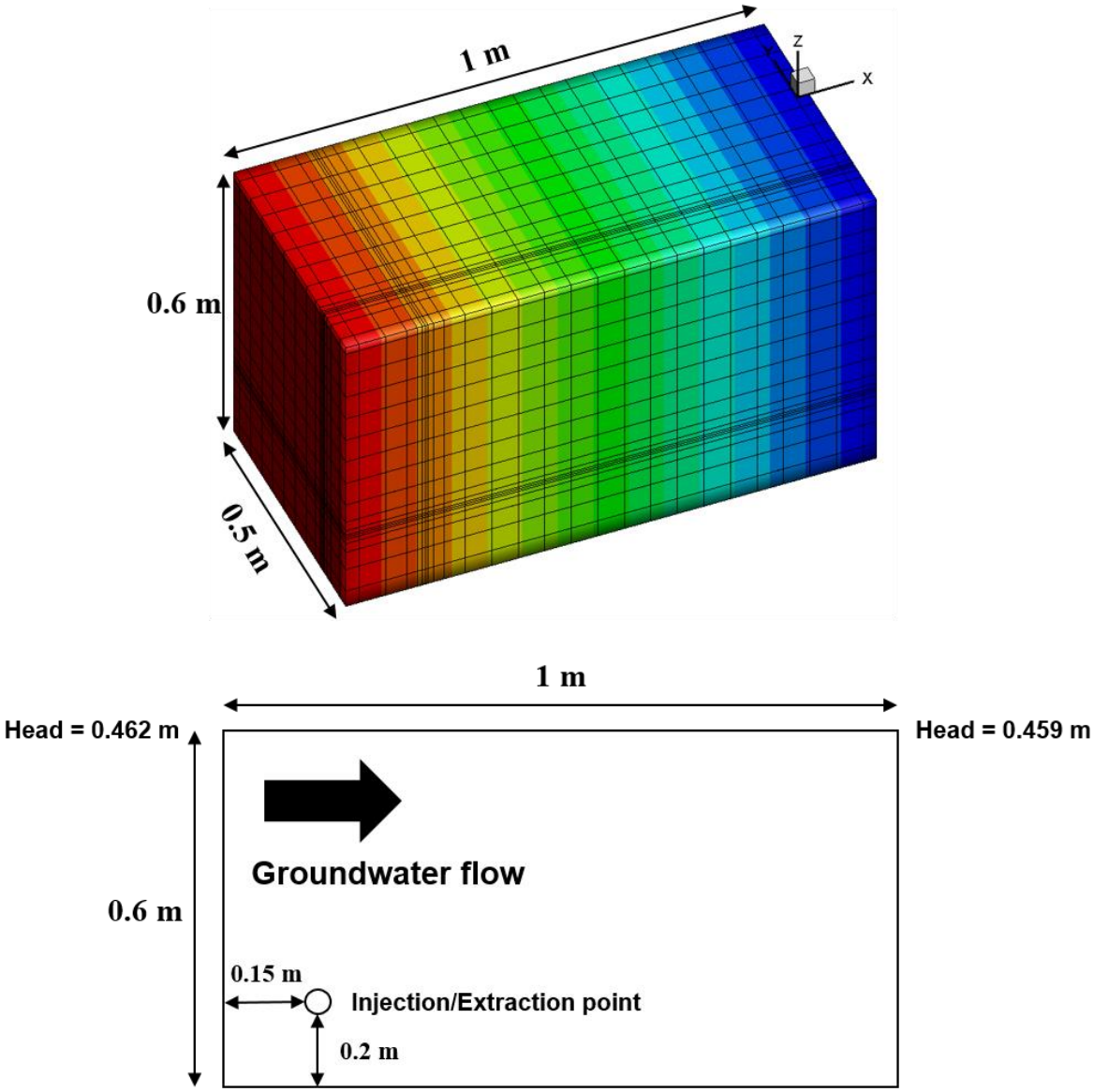

Fig. 3 - 6. Model domain and boundary condition for numerical simulation

Table 3 - 2 Model parameters for numerical simulation

Parameter	Value
Aquifer properties	
Aquifer K	2.5e-3 m/sec
Porosity	0.34
Specific storage	2.3e-4 m^{-1}
Longitudinal dispersivity	0.03 m
Transverse dispersivity	0.015 m
Vertical transverse dispersivity	0.015 m
Fluid properties	
Fluid density	998.23 kg/m^3
Fluid viscosity	1.00e-3 m^2/s
KBr diffusion coefficient (Shackelford and Daniel, 1991)	2.02e-9 m^2/s

3.2 Results and Discussions

3.2.1 Laboratory push-drift-pull tests under various conditions

Different drift times

The applied drift times were set to 3, 5, 8, and 10 min. The hydraulic gradient was set to 1.2 $\times 10^{-2}$. The applied KBr concentration was set to 160 mg/L, in order to prevent the density effect. The results of tests are shown in Fig. 7. The initial concentration of C/C_0 becomes lower as drift time increases. The first C/C_0 value of 3 min and 5 min was about 0.8, but it decreased to 0.36 in case of 8 min and 0.05 in case of 10 min. The reason of decreasing the initial C/C_0 is considered that the tracer plume dispersed during the drift times.

Different concentrations

The applied concentrations were set from 174 mg/L to 2450 mg/L and the hydraulic gradient was 3×10^{-3}. The applied drift times were 10 min under hydraulic gradient of 3×10^{-3}. When the concentration was 174 mg/L, the initial C/C_0 value showed the largest value of 0.51. However, with increasing the concentration of tracer (398 mg/L→1050 mg/L→2450 mg/L), the initial C/C_0 value showed decreasing trends (0.26 → 0.06 → 0.05). Istok and Humphrey (1995) investigated the density effect on breakthrough curve from two-well tracer tests with laboratory sand box experiments. The primary effect that the sinking tracer plume had on the breakthrough curve was to reduce the magnitude of the peak. The similar results from Istok and Humphrey (1995) that reducing the magnitude of the peak appeared in single well push pull tracer test from this study. It can be assumed that increasing the input tracer concentration of solution

intensified the sinking effect of the solute during the drift-phase, in which the injected tracer migrates with the ambient groundwater flow. For the circumstances of enhancing the density sinking effects for the drift time, the constant pumping rate regardless of the density incensement hardly capture the transported plume of the tracer for the pull phases entirely.

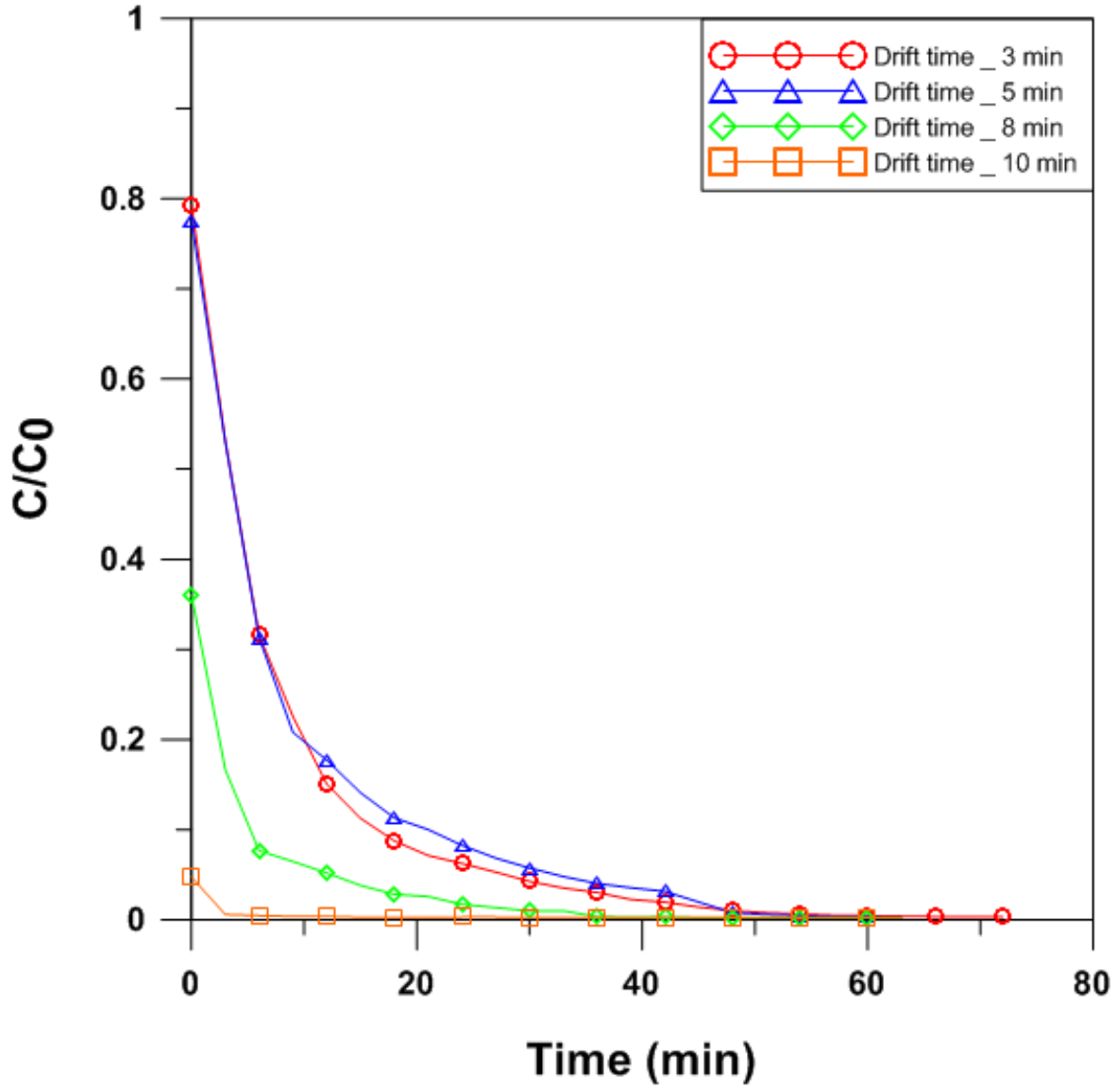

Fig. 3 - 7. Breakthrough curves under different drift times obtained from laboratory-scale push-drift-pull tracer tests (concentration: 160 mg/L, hydraulic gradient: 1.2×10^{-2})

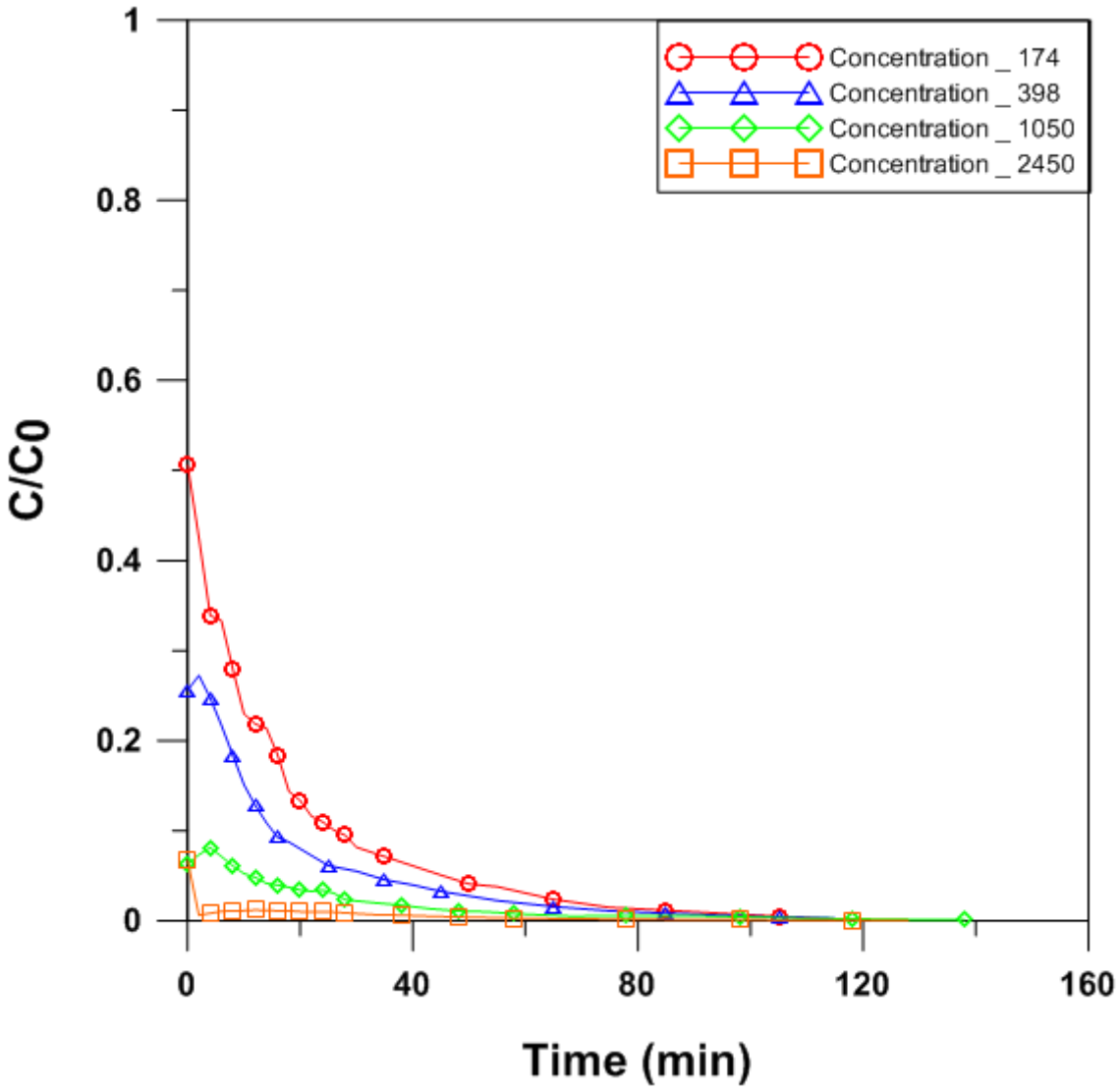

Fig. 3 - 8. Breakthrough curves under different tracer input concentrations obtained from laboratory-scale push-drift-pull tracer tests (drift time: 10 min, hydraulic gradient: 3.0×10^{-3})

Different hydraulic gradients

The results of the push-drift-pull tests under different hydraulic gradients are shown in Fig. 9. In order to investigate the impact of hydraulic gradient, the drift time was applied with the same condition as 5 min, and the concentration was applied under 238 mg/L, in order to prevent the density effect. The tested hydraulic gradients were 3×10^{-3}, 8×10^{-3}, and 1.2×10^{-2}. During the extraction phase, the initial value of C/C_0 was the highest when the hydraulic gradient was the lowest, and it decreased (0.35 → 0.28 → 0.14) while the hydraulic gradient was increasing. It can be estimated that the constant pumping rate regardless of the enhanced hydraulic gradient hardly capture the injected plume moved more than lower hydraulic gradient condition. Then, the injected plume the dispersion mechanism was activated.

Different penetrating depths

To investigate the effect of well penetrating depth, wells were positioned at the bottom, 10 cm above and 20 cm above from the bottom of sand tank. The applied drift time was 5 min, and the tracer concentration was under 160 mg/L. The results are shown in Fig. 10. The shape of breakthrough curves under various penetrating depths was nearly same. Also, the end time of pumping phase was similar. It indicates that the penetrating depth of well is not an important consideration in push-drift-pull test design, and the estimating linear velocity by push-drift-pull tracer test can be applied to partially penetrating wells under no-density effect condition.

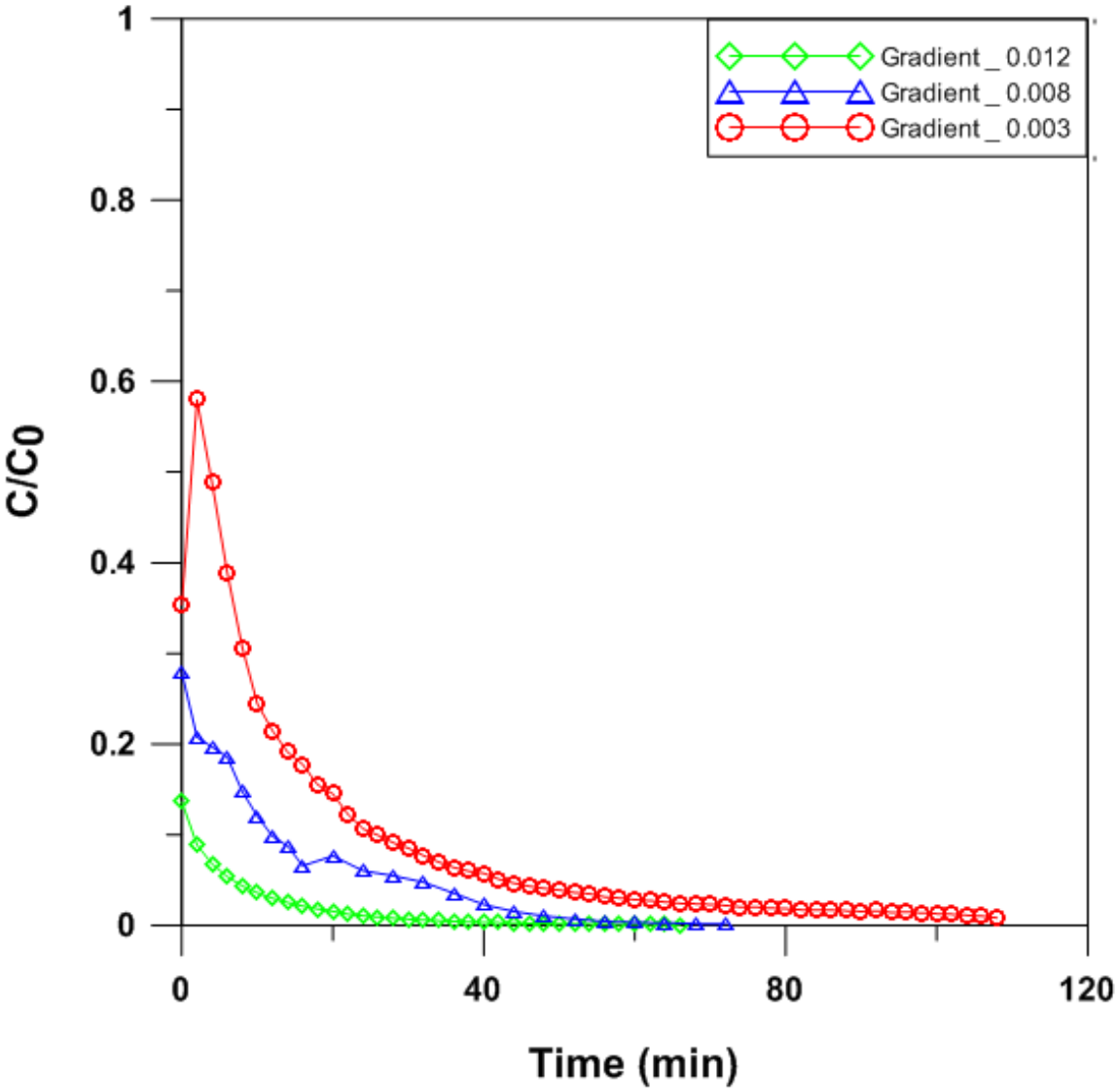

Fig. 3 - 9. Breakthrough curves under different hydraulic gradients obtained from laboratory-scale push-drift-pull tracer tests (concentration: 160 mg/L, hydraulic gradient: 3×10^{-3})

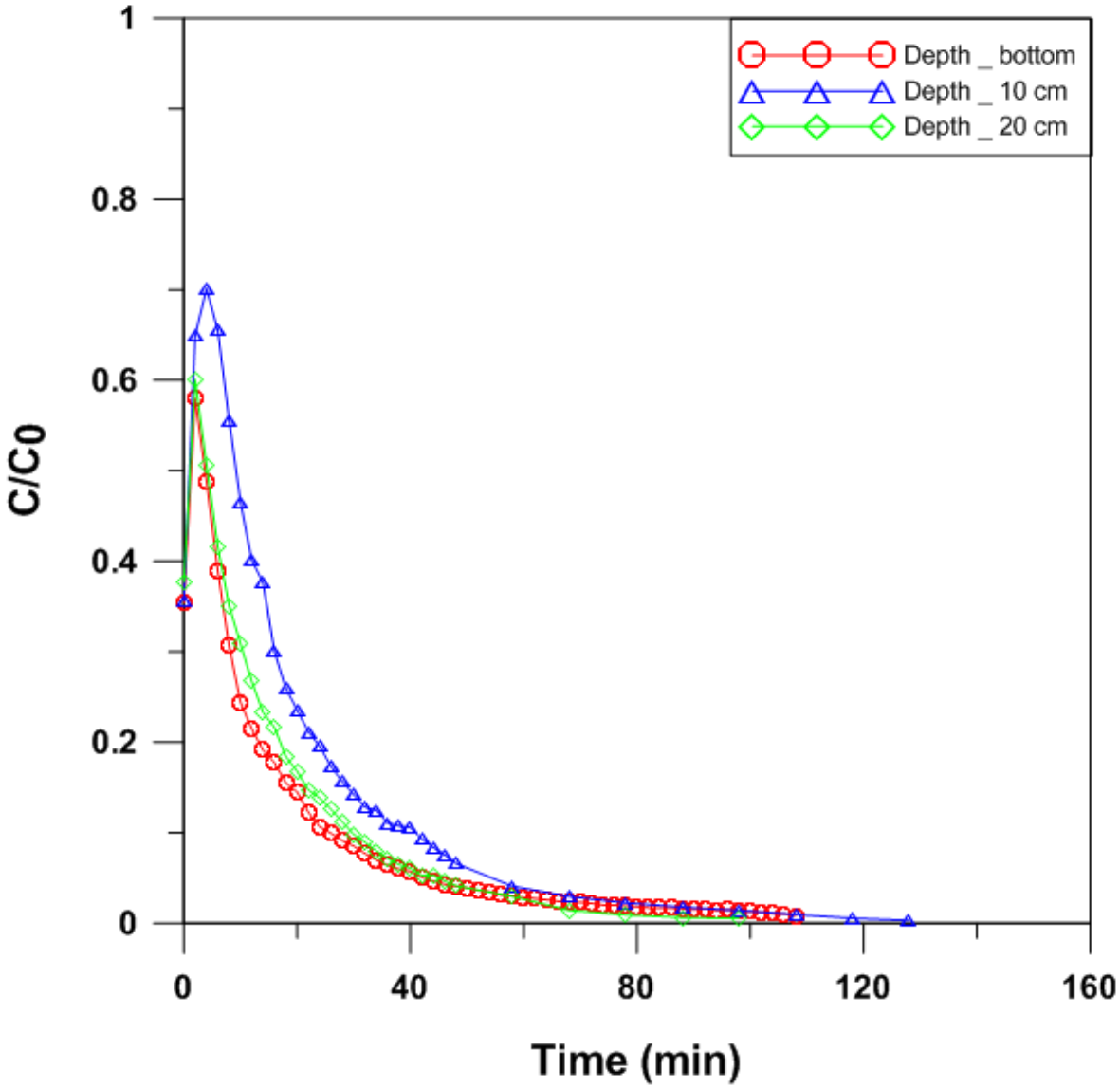

Fig. 3 - 10. Breakthrough curves under different well penetrating depths obtained from laboratory-scale push-drift-pull tracer tests (concentration: 160 mg/L, hydraulic gradient: 3×10^{-3}, and drift time: 5 min)

3.2.2 Sensitivity analysis

The sensitivity analysis was performed with controlled experimental conditions. The investigated conditions were drift time, tracer concentration, hydraulic gradient, and penetrating depth.

Sensitivity analysis was performed to figure out the important factor of push-drift-pull test and consider the factor during designing the tests. Sensitivity is the partial derivative of tracer concentration resulting from a change in a model parameter. (Knopman and Voss, 1987 and Harvey et al., 1996),

$$S_{ij} = \frac{\partial C_i}{\partial P_j}$$

where S_{ij} is the sensitivity of push-drift-pull tracer concentration at time i to the j th parameter, C_i is the detected concentration at time i, and P_j is the j th parameter. In sensitivity analysis, the sign (positive or negative) is not important. The absolute value of sensitivity indicates the sensitivity to the parameter. In this study, several experimental data handled in 3.2.1 were analyzed with sensitivity analysis to quantify the impact of parameters in time and provide the insight of single well push-drift-pull tracer test design.

Sensitivity to drift time

The used conditions for analyzing sensitivity to drift time were 10 ml/min of extraction rate, 15 cm/min of hydraulic conductivity, 160 mg/L of tracer concentration, and 3×10^{-3} of hydraulic gradient. Fig. 11. shows the sensitivity to drift time values at each elapsed time. The compared drift times were 3, 5, and 10 min. When the compared drift times were low (3 vs 5 min), the sensitivity values had no trend and showed low absolute value in all time. It can be assumed

that the gap of 2 min cannot cause the difference of breakthrough, but the sensitivity values of early part increased with increasing of the drift time. It indicates that the drift time impacts the early part of breakthrough curves. It denotes that the sampling interval of the early part of test should be short enough to be short during pull phase with increasing of the drift time.

Sensitivity to tracer concentration

The used conditions for analyzing sensitivity to tracer concentrations were 10 ml/min of extraction rate, 15 cm/min of hydraulic conductivity, 10 min of drift time, and 3×10^{-3} of hydraulic gradient. The compared tracer concentrations were 174, 398, and 1050 mg/L. In Fig. 12, the sign of sensitivity to tracer concentration was negative in almost of time. It indicates that the detected tracer concentration during pull phase showed decreasing trend with increased input tracer concentration. The absolute values of sensitivity to tracer concentrations were high in early part of breakthrough curves. It illustrates that the sampling interval of the early part of test should be short enough during pull phase as tracer concentration is increasing.

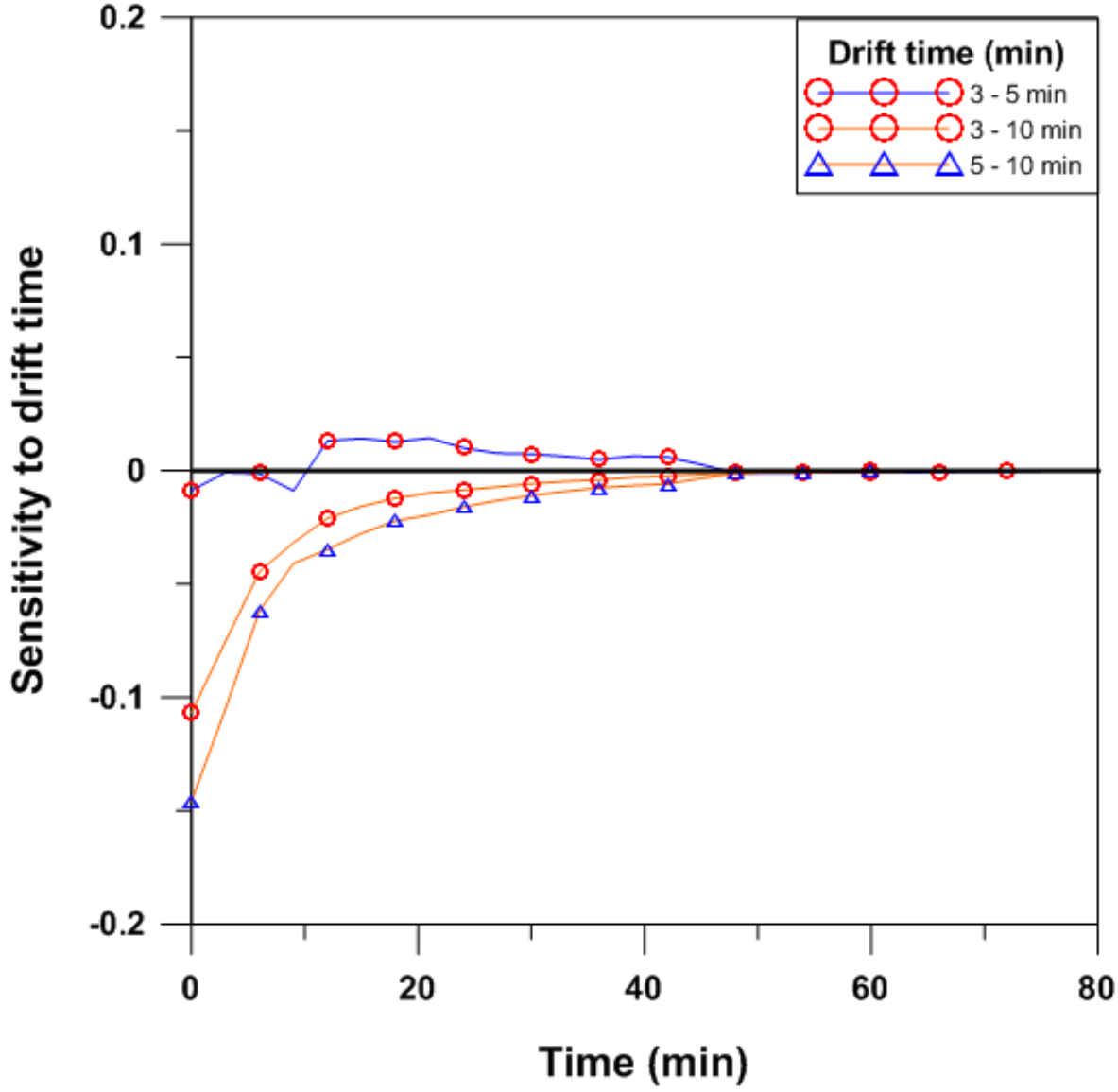

Fig. 3 - 11. Results of sensitivity analysis in time with 3 cases of different drift time (3 min, 5 min, and 10 min)

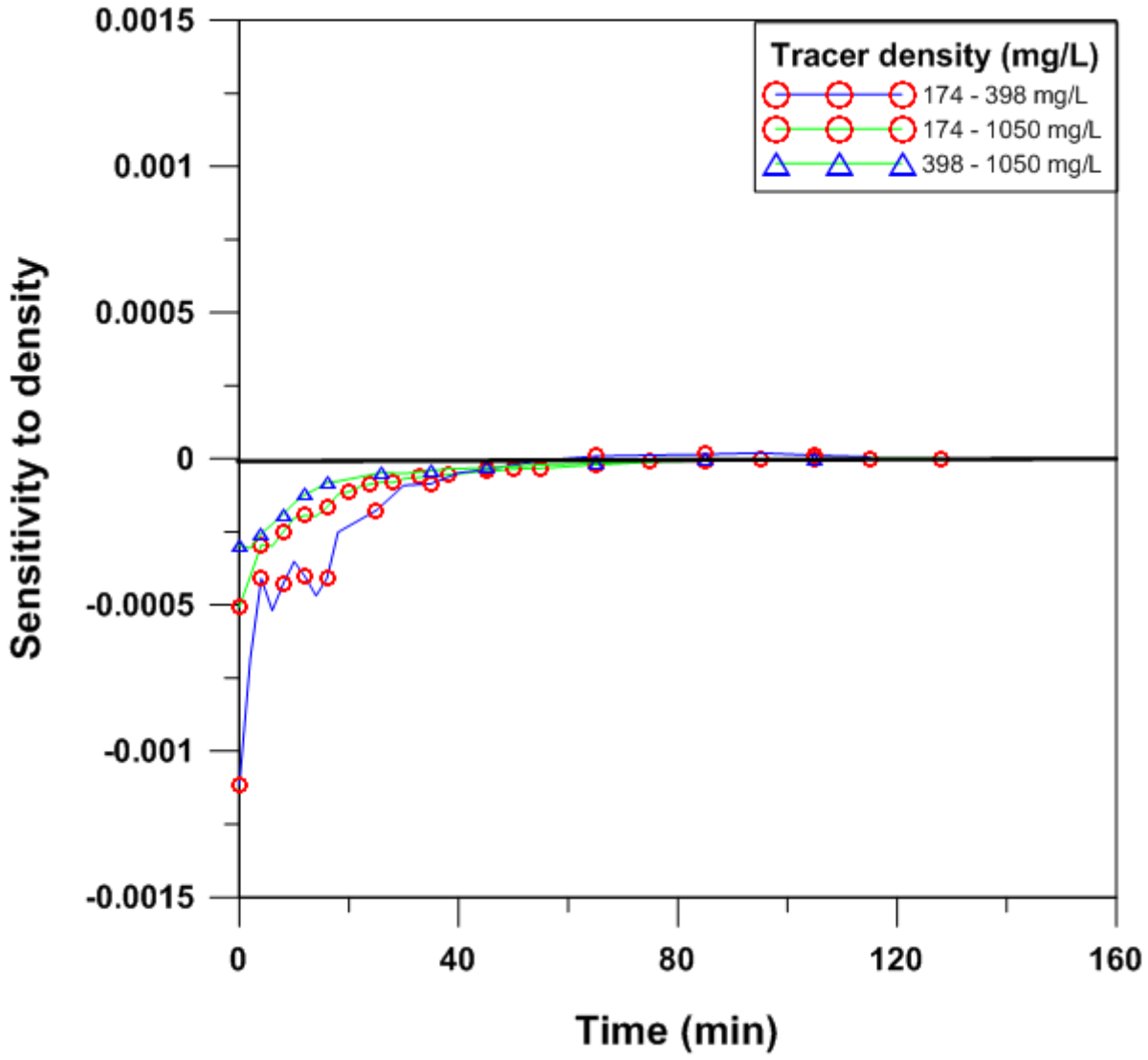

Fig. 3 - 12 Results of sensitivity analysis in time with 3 cases of different input concentration (174 mg/L, 398 mg/L, and 1050 mg/L)

Sensitivity to hydraulic gradient

Applied conditions for analyzing sensitivity to hydraulic gradient were 10 ml/min of extraction rate, 15 cm/min of hydraulic conductivity, 5 min of drift time, and 160 mg/L of tracer concentration. The applied hydraulic gradients were 3×10^{-3}, 8×10^{-3}, and 1.2×10^{-2}. In Fig. 13, the sign of sensitivity to hydraulic gradient was negative in early time. It indicates that the detected tracer concentration during pull phase showed decreasing trend with increased hydraulic gradient. The larger sensitivity values were obtained from early time of all cases and they decreased as elapsed time increases. It indicates that increasing hydraulic gradient can affect the early part of breakthrough curve, and the end of pumping phase and the sampling interval should be short in early time.

Sensitivity to penetrating depth

To investigate the sensitivity to penetrating depth, the experimental conditions were set identical except the penetrating depth of well. The extraction rate was 10 ml/min and the hydraulic conductivity was 15 cm/min. Additionally, 5 min of drift time and 160 mg/L of tracer concentration were applied. The acryl wells were positioned at the bottom, 10 cm above and 20 cm above from the bottom of sand tank, to make a different penetrating condition. The results derived from sensitivity to penetrating depth illustrated that there were no special trend (Fig. 14). The sign of sensitivity value was positive in case of 0 VS 10 cm and negative in case of 10 VS 20 cm. But, the absolute values of sensitivity were nearly zero in all time when the gap of penetrating depth was the biggest case (0 vs 20 cm). It indicates that the penetrating depth of well doesn't affect the entire part of breakthrough curves.

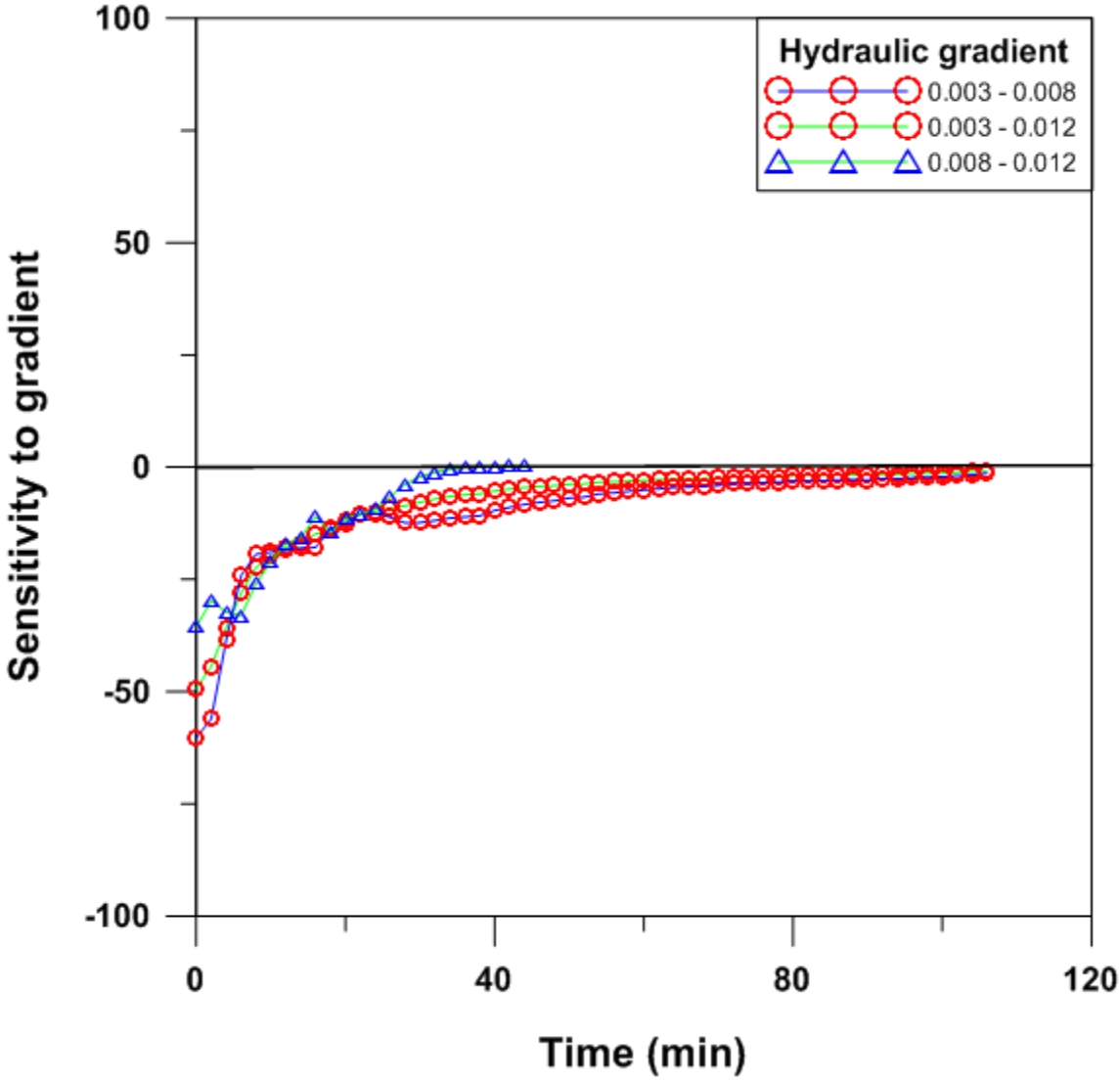

Fig. 3 - 13. Results of sensitivity analysis in time with 3 cases of different hydraulic gradient (3×10^{-3}, 8×10^{-3}, and 1.2×10^{-2})

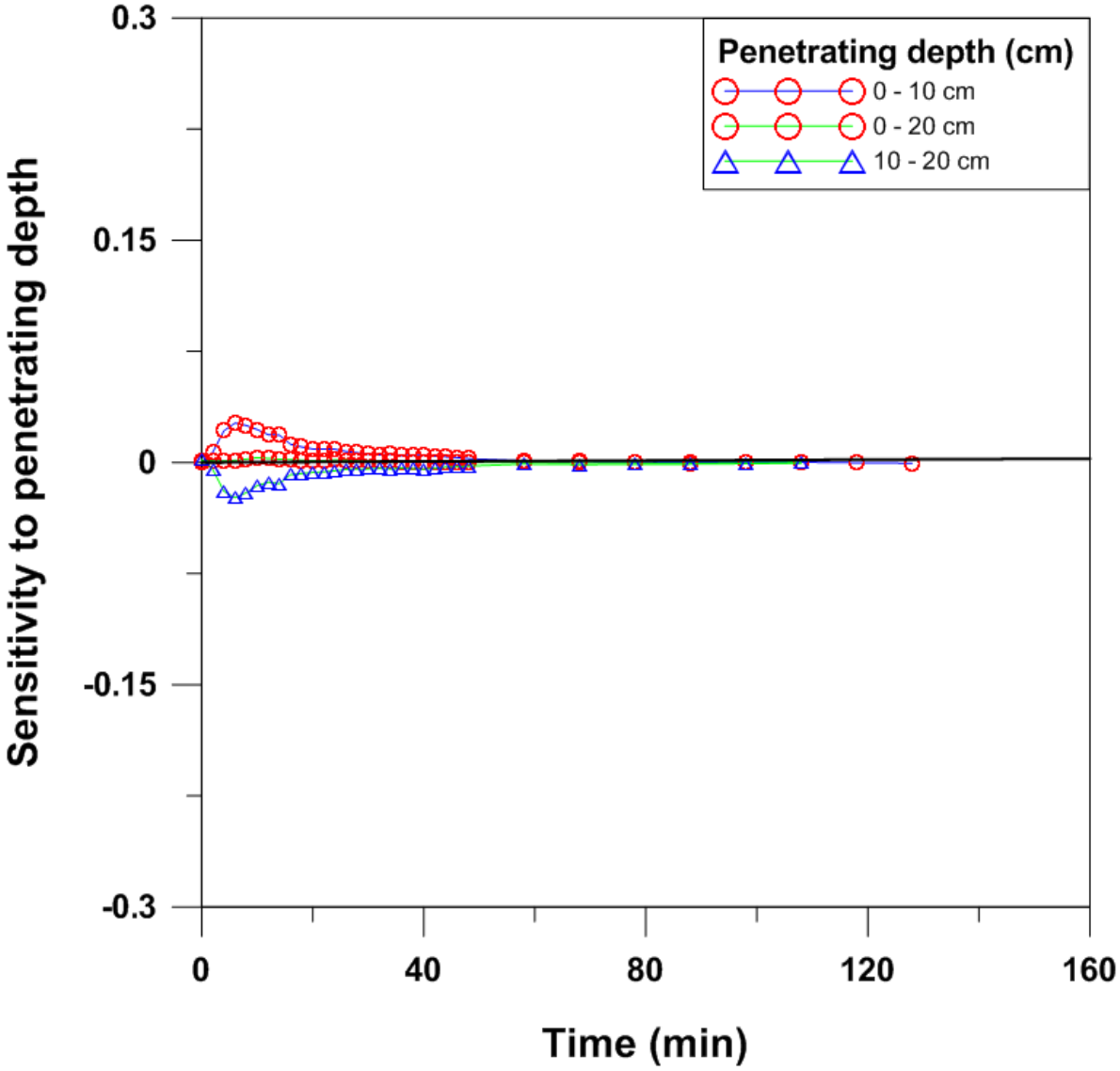

Fig. 3 - 14. Results of sensitivity analysis in time with 3 cases of different well penetrating depth (0 cm, 10 cm, and 20 cm above from the bottom)

3.2.3 Numerical simulations with various concentrations and pumping rates

Density effect on push-drift-pull tracer tests in terms of estimating linear velocity

The experimental results were used to calibrate the numerical model. Three different experimental conditions were used to validate numerical model (no-density effect condition A, density-induced sinking condition B and C). In A condition, the Root Mean Square Error (RMSE) was 0.04. In B, C conditions, the values of RMSE were 0.057 and 0.017, respectively (Fig. 15). After validation, several case studies were simulated to verify the density effect on push-drift-pull tracer test.

To investigate the change of t_{com} with increasing the input tracer concentration, several simulations were conducted with various drift times, and the results are shown in Fig. 16. The pumping rate of all simulations were applied as 78 ml/min to estimate the linear velocity value of no-density condition (160 mg/L in case A) similar to the Darcy velocity. The linear velocity values of no-density condition (160 mg/L) in case B and C were underestimated compared with the value of case A (160 mg/L). It can be assumed that the dispersion was intensified as travel distance was longer than before (20 min of drift time) during lengthen drift time. They caused the hardly capture of injected plume with constant pumping rate and the linear velocity values were underestimated and the results have same trend of Hwang's study (2002). When the concentration of tracer increased, the value of t_{com} also increased. It can be explained that the injected tracer plume traveled far from the well while t_{com} was increased during the same resting

time. It means the velocity should be estimated higher when the input concentration of tracer is increasing. However, Fig. 16 showed that the estimated linear velocity was decreased as the concentration of tracer was increasing. Increased tracer concentration was intensified with applying the increased drift time. Because the Hall's equation (Eq. 2-2) estimates the linear velocity, the horizontal travel distances of each case were plotted in Fig. 17. The horizontal travel distance can be derived as:

$$\text{Horizontal travel distance L} = \text{V} \times t_{com} \quad \text{(Eq. 3-5)}$$

Where V is a linear velocity; and t_{com} is a time of center of mass at each input concentration condition. In Fig. 17, the horizontal distance values for estimating Darcy velocity were compared with the real traveled horizontal distance values. Specifically, to draw the Darcy velocity value (0.14 cm/min) at the concentration condition of 398 mg/L, the horizontal travel distance should be calculated as 0.14 cm/min (Darcy velocity) × 48.4 min (t_{com} of 398 mg/L condition). Finally, the value for estimating Darcy velocity is 6.8 cm. However, the real traveled horizontal distance can be calculated as 0.12 cm/min (estimated from Eq. 2-2 under density effect condition of 398 mg/L) × 48.4 min (t_{com} of 398 mg/L condition) and the result is 6.0 cm. The results indicate that the real horizontal travel distance can be estimated less than the horizontal distance values for estimating Darcy velocity. In other words, underestimated linear velocity can be obtained in density effect condition.

The conceptual model of estimating linear velocity was made to know the decreasing trend

of linear velocity, according to the no-density and density cases (Fig. 18). If the tracer plume traveled horizontally along with the groundwater flow direction without density-induced sinking effect, it can provide a good estimation of linear velocity (A). However, tracer density can affect the flow route and the sank during transportation (B). In other words, in case (B), the horizontal travel distance of tracer plume in porous media is shorter than case (A) ($L_1 > L_2$), and the estimated linear velocity can be decreased.

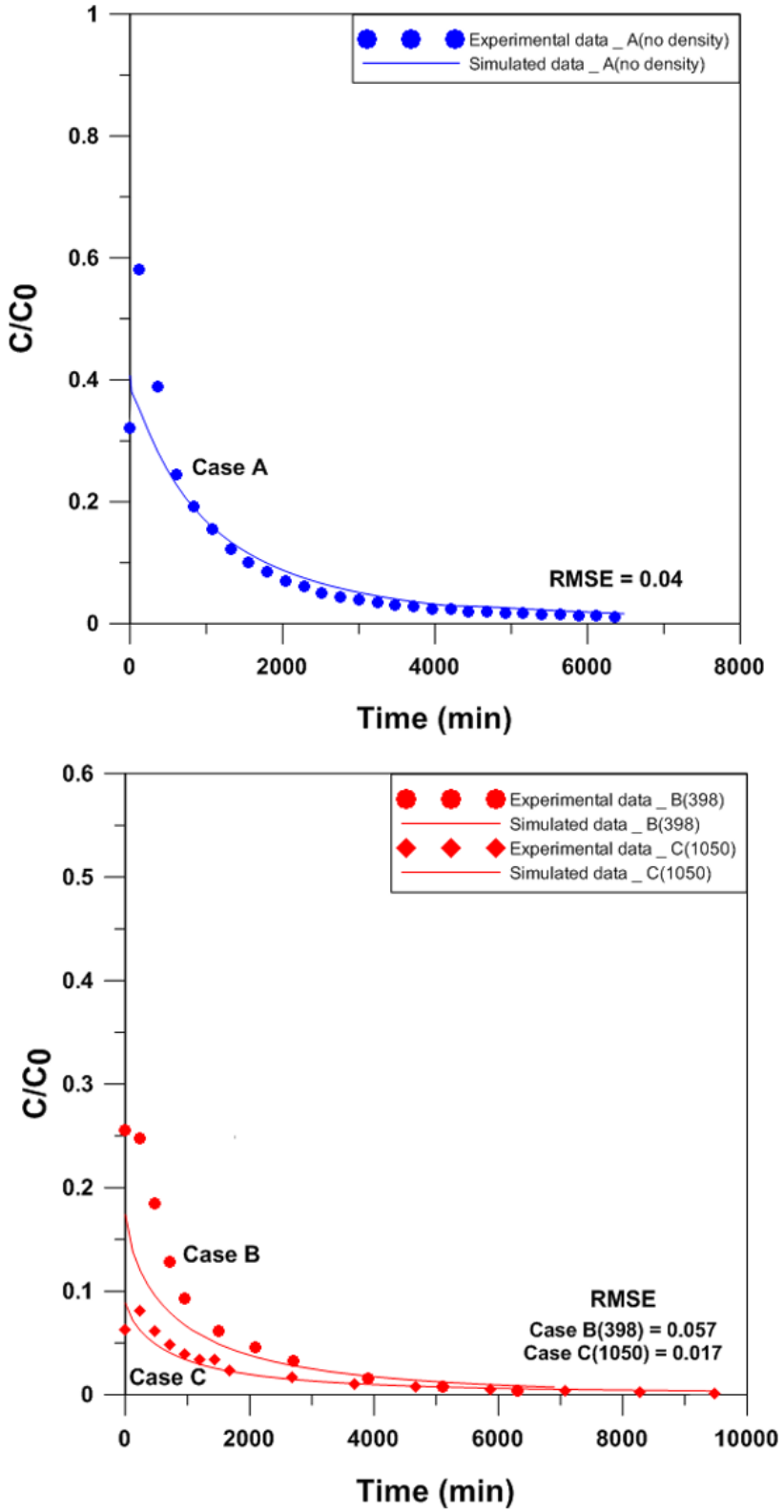

Fig. 3 - 15. Comparison of the C/C_0 value obtained from the numerical simulation (in full line) with that from the experiments (in dot) with 3 density conditions: (A) 160 mg/L, (B) 398 mg/L, (C) 1050 mg/L.

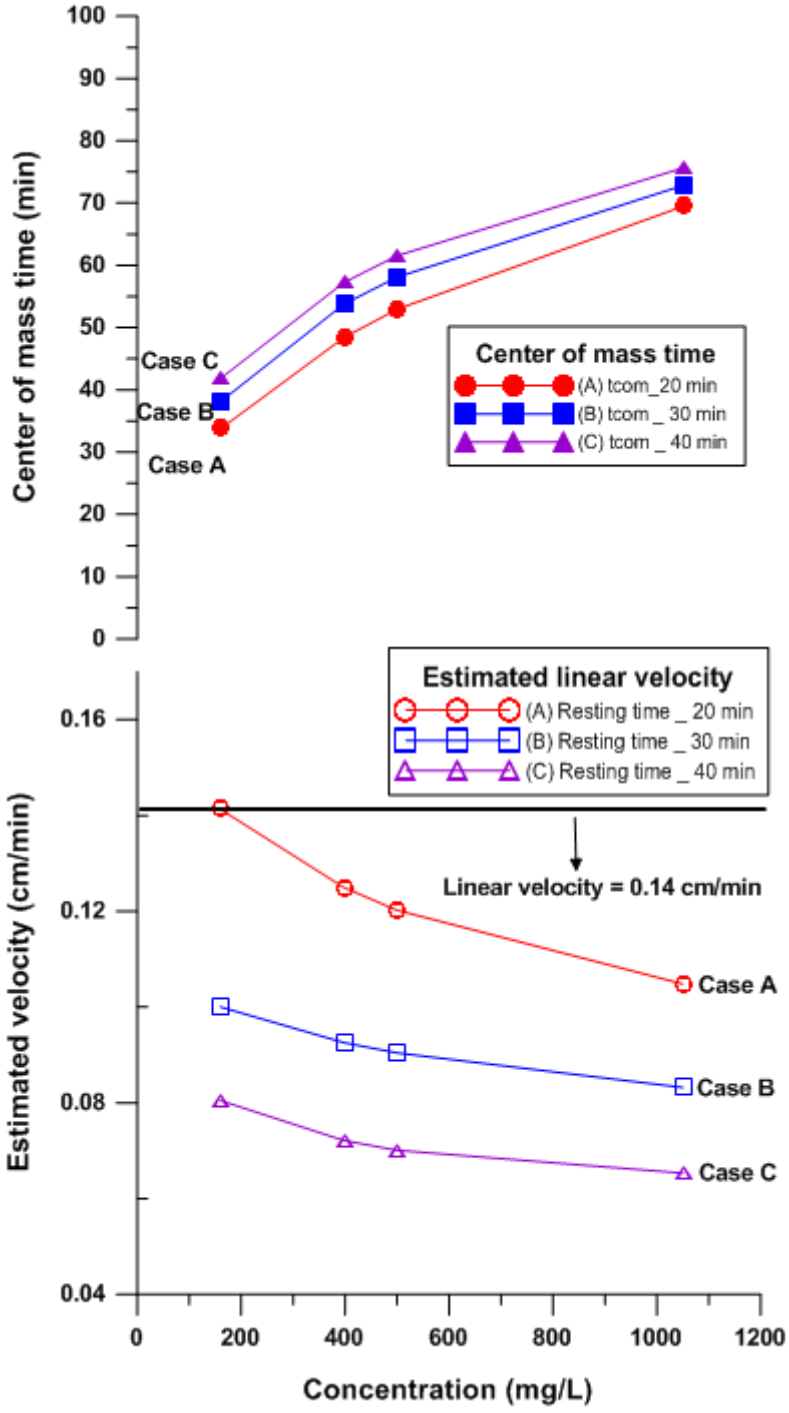

Fig. 3 - 16. Center of mass time (t_{com}) and estimated linear velocity from the varied input tracer concentration for 12 cases.

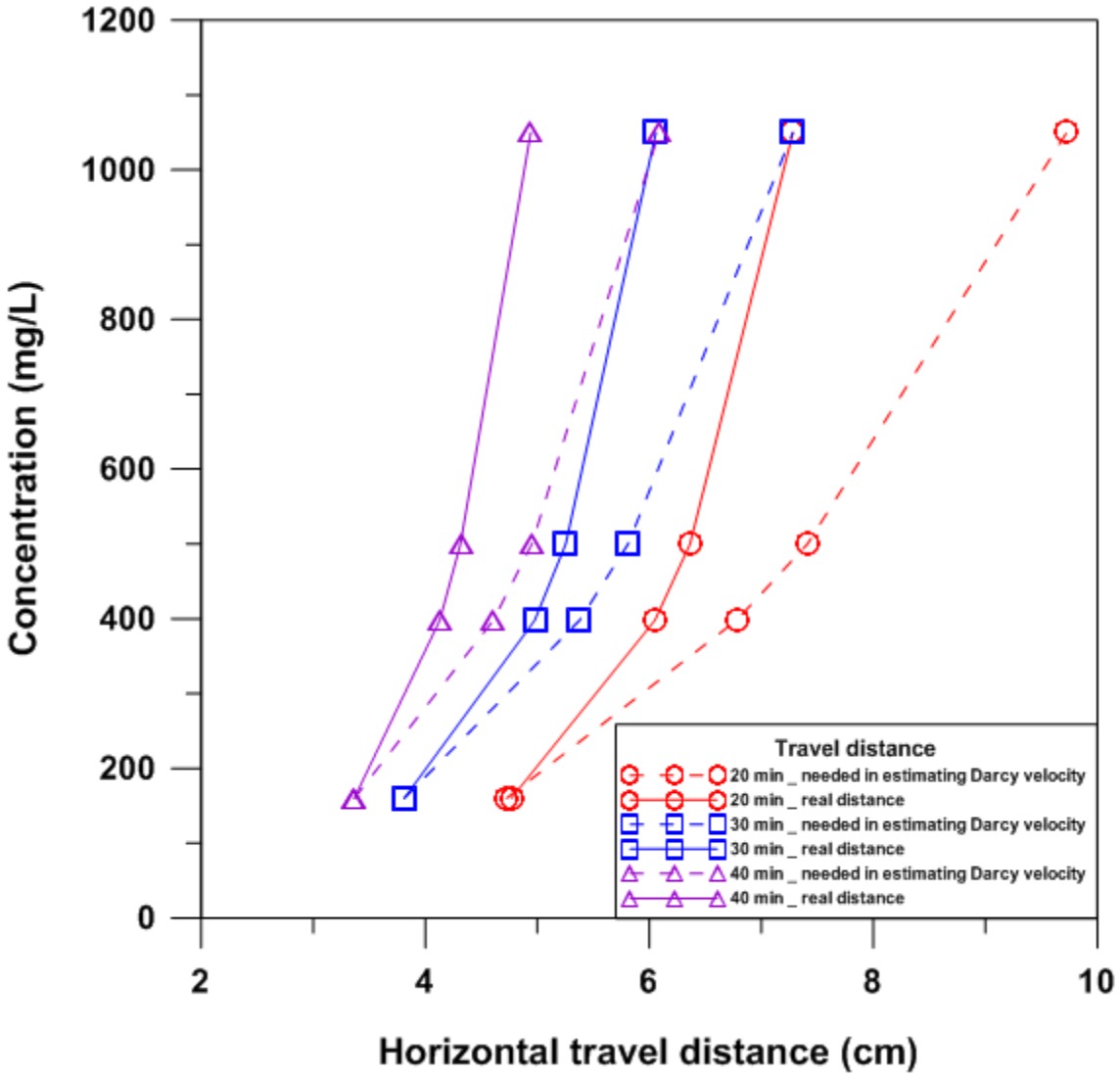

Fig. 3 - 17. The comparison of the horizontal distance values needed in estimating Darcy velocity with the real horizontal distance values in various density conditions.

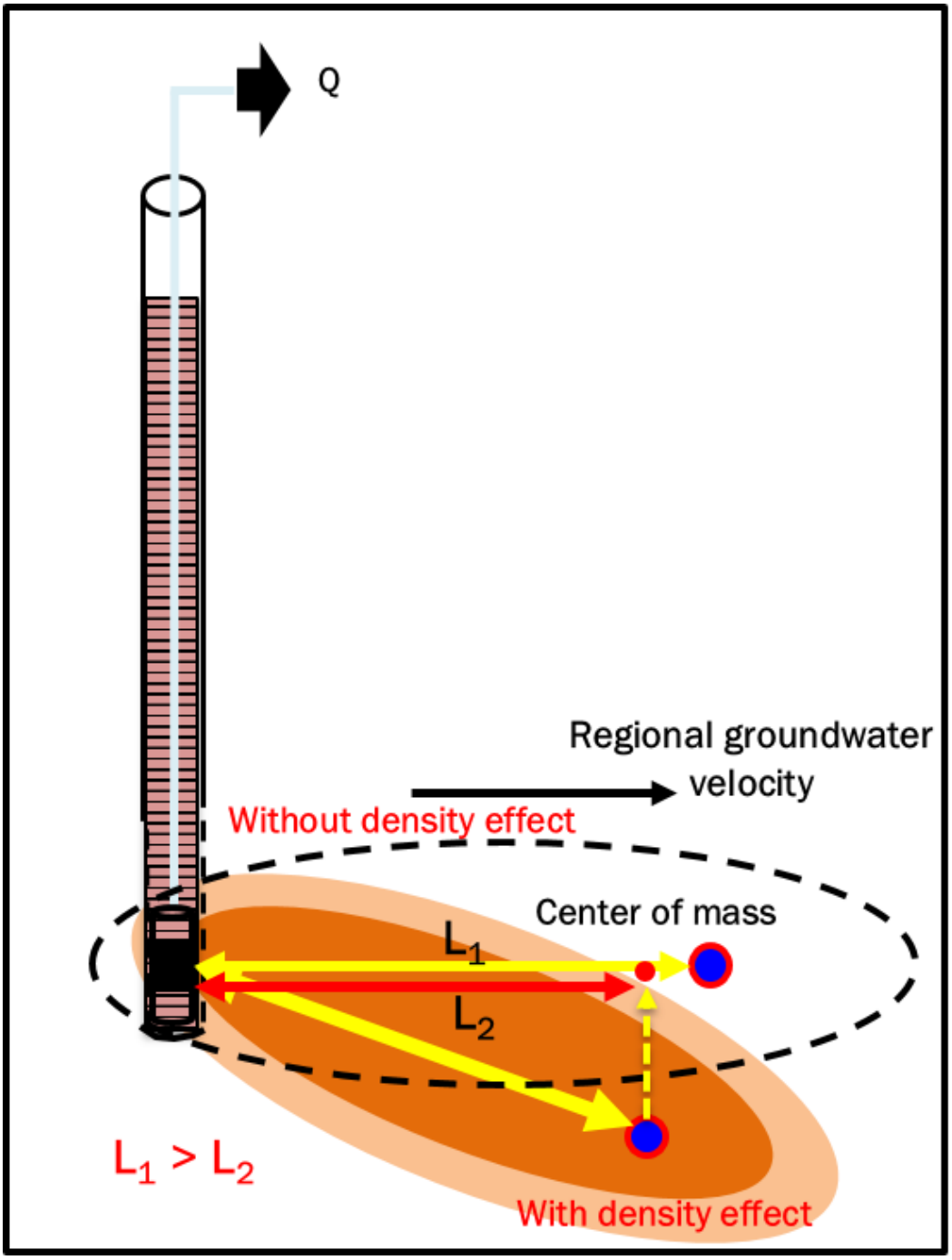

Fig. 3 - 18. The conceptual model of migration of tracer plume under no-density effect condition and density effect condition (L_1: horizontal distance of no-density case, L_2: horizontal distance of density case).

Estimating pumping rate Q under various background velocity

As the result of the experiment, the estimated linear velocity was lower than the Darcy velocity (seepage velocity) due to the low pumping rate. To enhance the estimated velocity similar to the Darcy velocity, increased pumping rate of 60 ml/min was simulated by numerical model, and the influence of pumping rate is shown in Fig. 19. The linear velocity values obtained from applying increased pumping rate were higher than the Darcy velocity. It indicates that appropriate pumping rate is important to estimate the exact linear velocity. The background groundwater flow rates are different, according to sites or test conditions, various flow conditions were simulated to investigate the effect of pumping rate at each condition. The applied hydraulic gradients were increased from 5×10^{-4} to 7×10^{-3} in simulations, and proper pumping rates at each background flow condition are plotted in Fig. 20.

Fig. 20 shows that reasonable pumping rate was enhanced while the background groundwater flow rate was increasing. In addition, 500 mg/L of tracer concentration condition was also applied to investigate the reasonable pumping rate under density effect condition. In this case, higher pumping rate was required in case of denser plume than no-density effect condition. As mentioned above, density effect can cause the underestimation of linear velocity and the results supported that the demand of higher pumping rate under density-effect condition is reasonable. Therefore, when there is density-induced sinking effect, the pumping rate needed to be enhanced to obtain the more reliable linear velocity value and the difference of reasonable

pumping rate between no-density case (160 mg/L) and density-effect case (500 mg/L) became larger with increasing the background groundwater flow rate.

Fig. 21 represents the comparison between the theoretical capture zone and estimated capture zone obtained from numerical simulations. The injected tracer plume will be advected along with the flowing groundwater so the distance of the center of mass from the injection point could be calculated as $x = v_x t$. In addition, the injected plume will be dispersed by groundwater flow. For this reason, a normal or Gaussian distribution of the standard deviation of the distribution should be used to estimate the distribution of tracer in the plume. The equation is given by (Fetter, 1999):

$$\sigma_x = \sqrt{2D_L t} \qquad \text{(Eq. 3-6)}$$

Where D_L is a hydrodynamic dispersion coefficient that is parallel to the principal direction of flow; t is a travel time. By adding the distribution of tracer in recovery rate of each test to the position of center of mass of plume, the theoretical capture zone can be calculated. The estimated capture zone in an unconfined aquifer can be calculated by the position of the stagnation point – that is, the down-gradient end of the capture zone – given by (Grubb, 1993):

$$x = \frac{QL}{\pi K({h_1}^2 - {h_2}^2)} \qquad \text{(Eq. 3-7)}$$

Where Q is a pumping rate; L is a distance between the two observation points; h_1 is an up-gradient head between two observed head; h_2 is a down-gradient head between two observed

head; and K is a hydraulic conductivity. The pumping rate Q in Eq. 3-7 was calculated from the numerical simulation (Fig. 20), which was reasonably estimated to obtain the exact linear velocity. The two observation points were set at (0.05, 0.1, 0.2) and (0.5, 0.1, 0.2) of (x, y, z) coordinate system. The up-gradient head value was obtained from the result of simulation at x = 0.05 m and the down-gradient head value was obtained from the result of simulation at x = 0.5 m. The results between the theoretical and estimated capture zone showed R-squared value of 0.93.

To confirm the difference of estimated linear velocity under higher and lower than the reasonable pumping rate (Q) derived above (Fig. 20), two cases of simulations were performed with half of the pumping rate (0.5Q) and twice of the pumping rate (2Q). Fig. 22 shows that higher than Q can cause overestimated linear velocity, and lower than Q can cause underestimated linear velocity. The conceptual model is shown in Fig. 23. When the applied pumping rate is low, only one part of total injected plume could be recovered because of small capture zone and the position of center of mass that can be calculated near the pumping well. The incorrectly calculated center of mass can cause the underestimated linear velocity. Contrary to low pumping rate, high pumping rate can enhance the recovery of plume and size of capture zone. Since pumping rate is the most sensitive parameter in Eq. 2-2, finding reasonable pumping rate is necessary. If pumping rate is too fast, the linear velocity can be overestimated.

The simulated results are shown in Fig. 24 (160 mg/L) and Fig. 25 (500 mg/L). In cases of applying low pumping rate (10 ml/min) same as the experiments, both cases showed a lot of residual (80 ~ 85% of injected mass) in flow field and underestimated linear velocity values were estimated because of low pumping rate. However, in case of applying reasonable pumping rate (50 ml/min in case of 160 mg/L and 66 ml/min in case of 500 mg/L, respectively) obtained from Fig. 20, both cases showed much less than residual (36 ~ 40% of injected mass) in flow field and the exact linear velocity values were estimated. Furthermore, density-induced sinking affected the tracer mass recovery rate. About 12% of injected tracer mass was recovered under density effect condition, while 20% of injected tracer mass was recovered without density effect condition. Both experiment had the same pumping rate of 10 ml/min. Consequently, the higher pumping rate should be applied under density effect condition to obtain the reliable linear velocity.

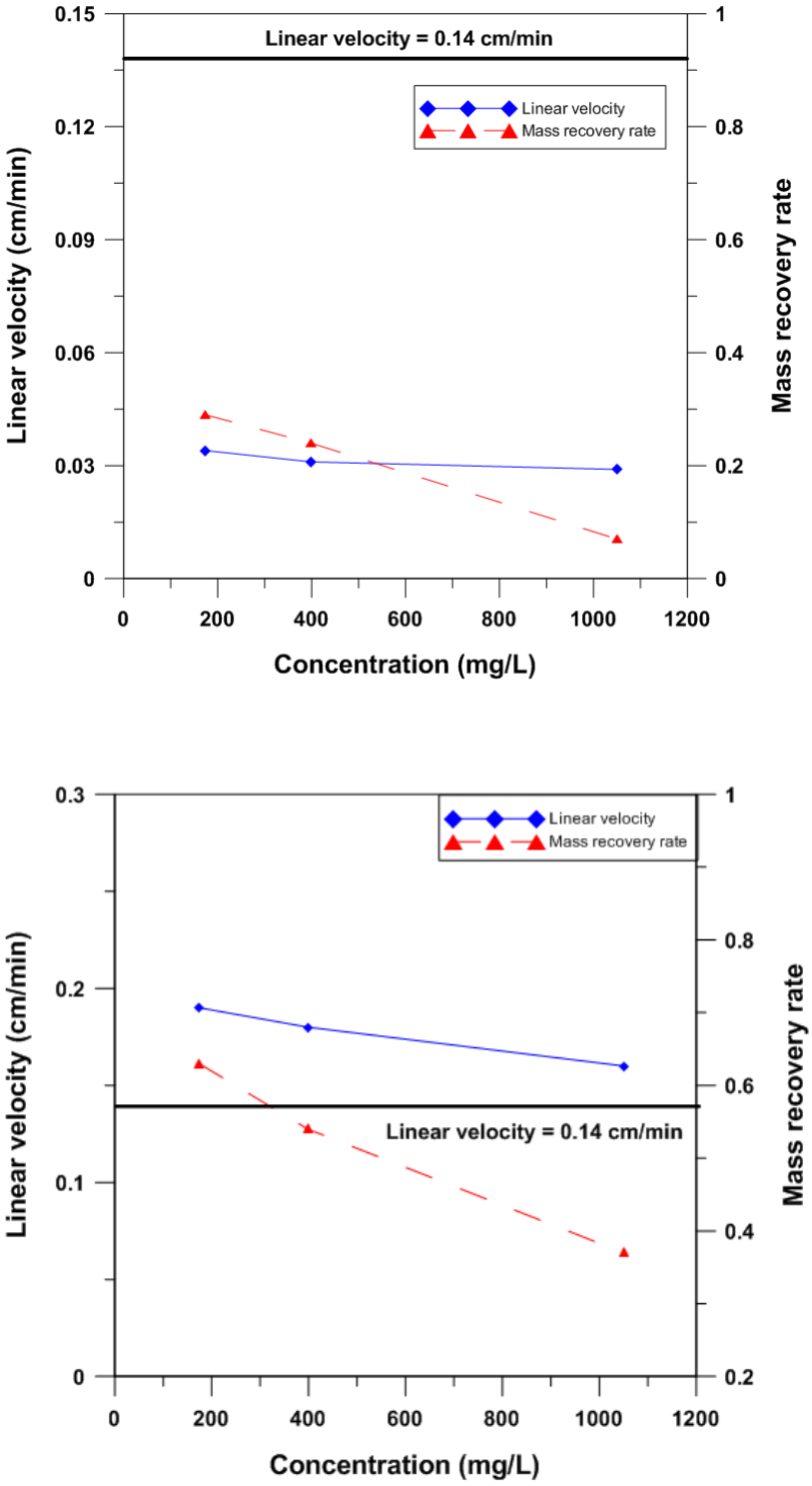

Fig. 3 - 19. The estimated linear velocity obtained from experiment (top) and numerical simulation (bottom) under different applied pumping rate: 10 ml/min (top) and 60 ml/min (bottom).

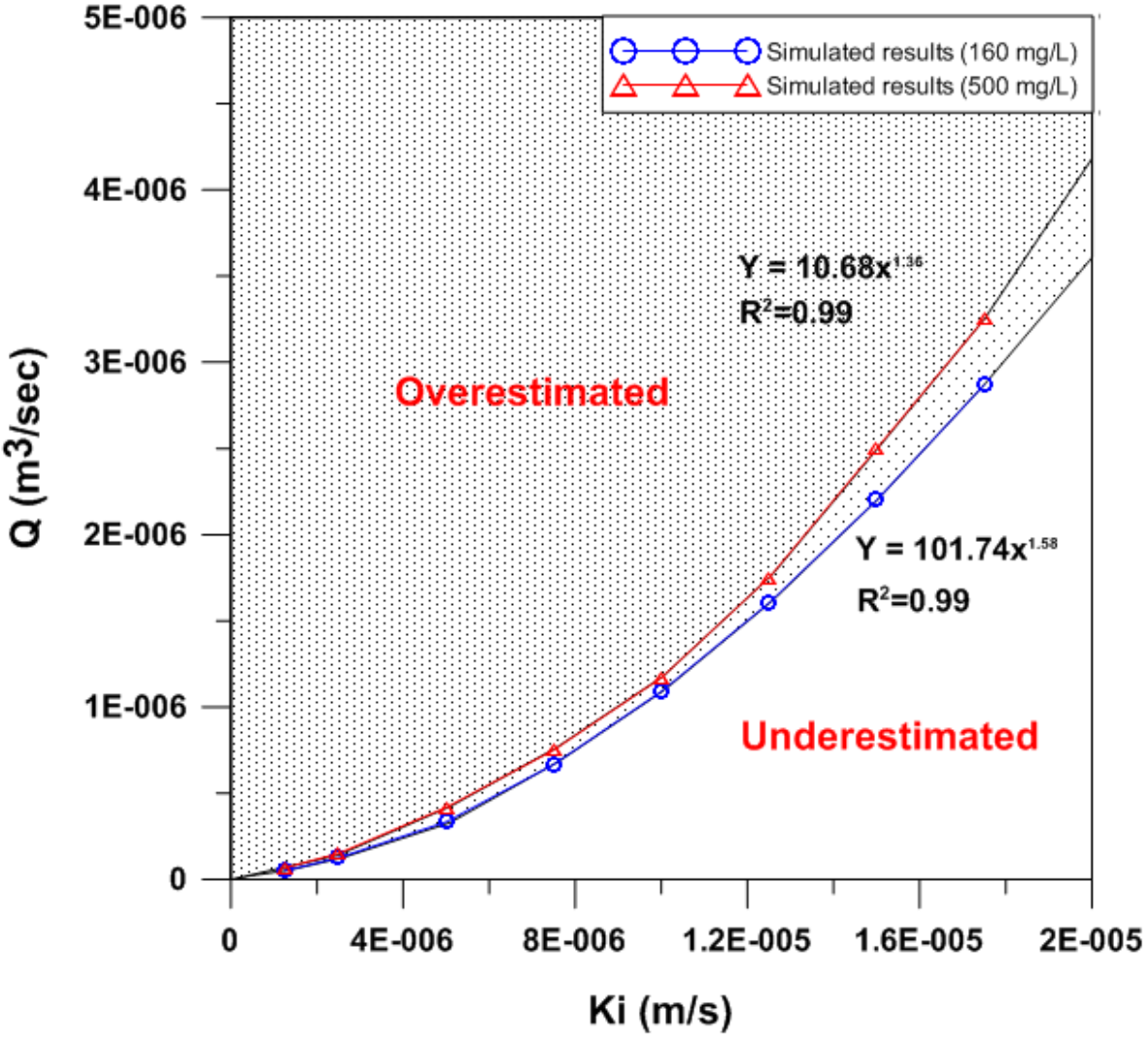

Fig. 3 - 20. The obtained reasonable pumping rates under various background groundwater velocity conditions for 2 concentration cases: 160 mg/L (in triangle) and 500 mg/L (in circle).

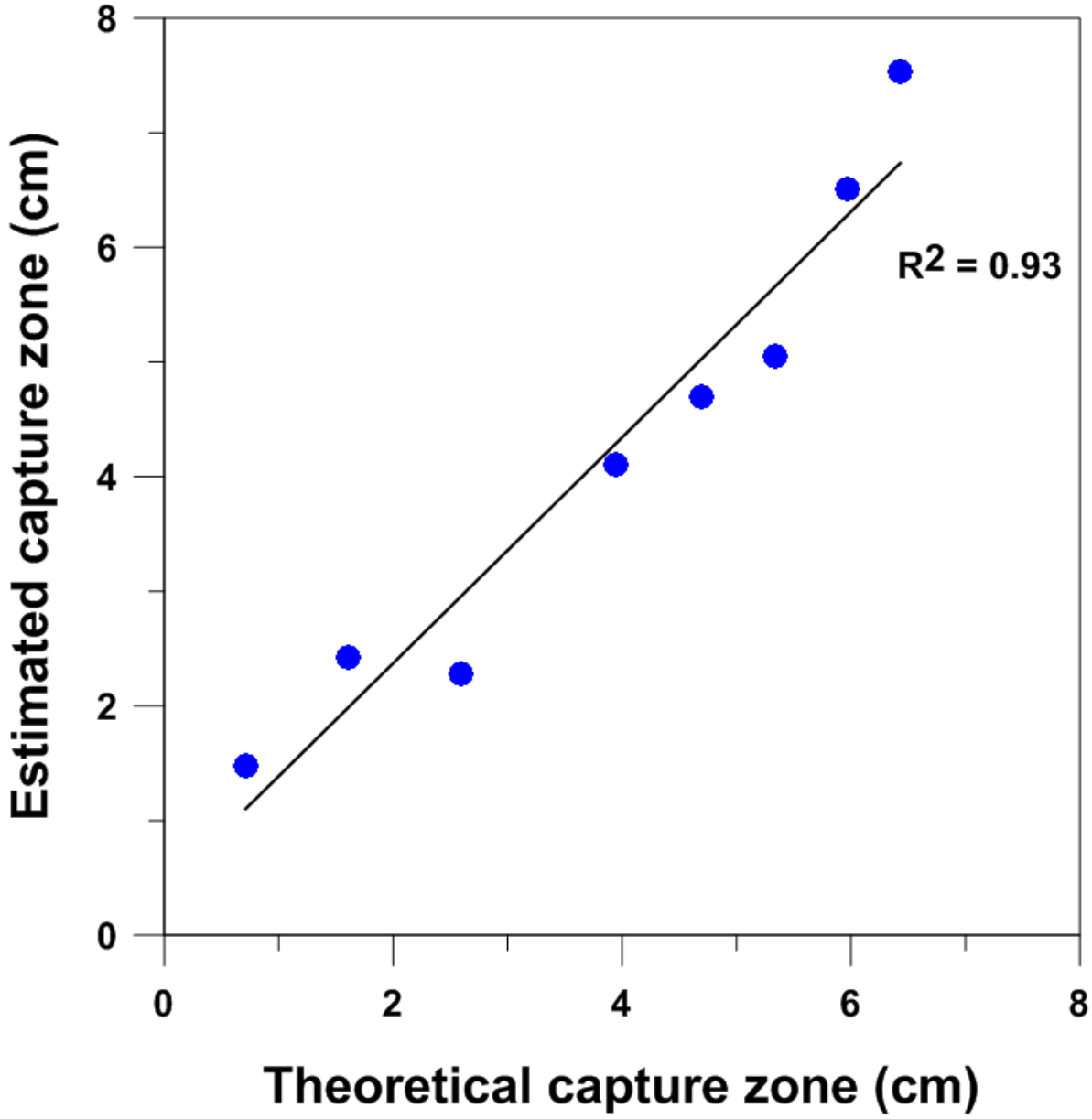

Fig. 3 - 21 The comparison between the theoretical capture zone and estimated capture zone by numerical simulations (R^2 = 0.93).

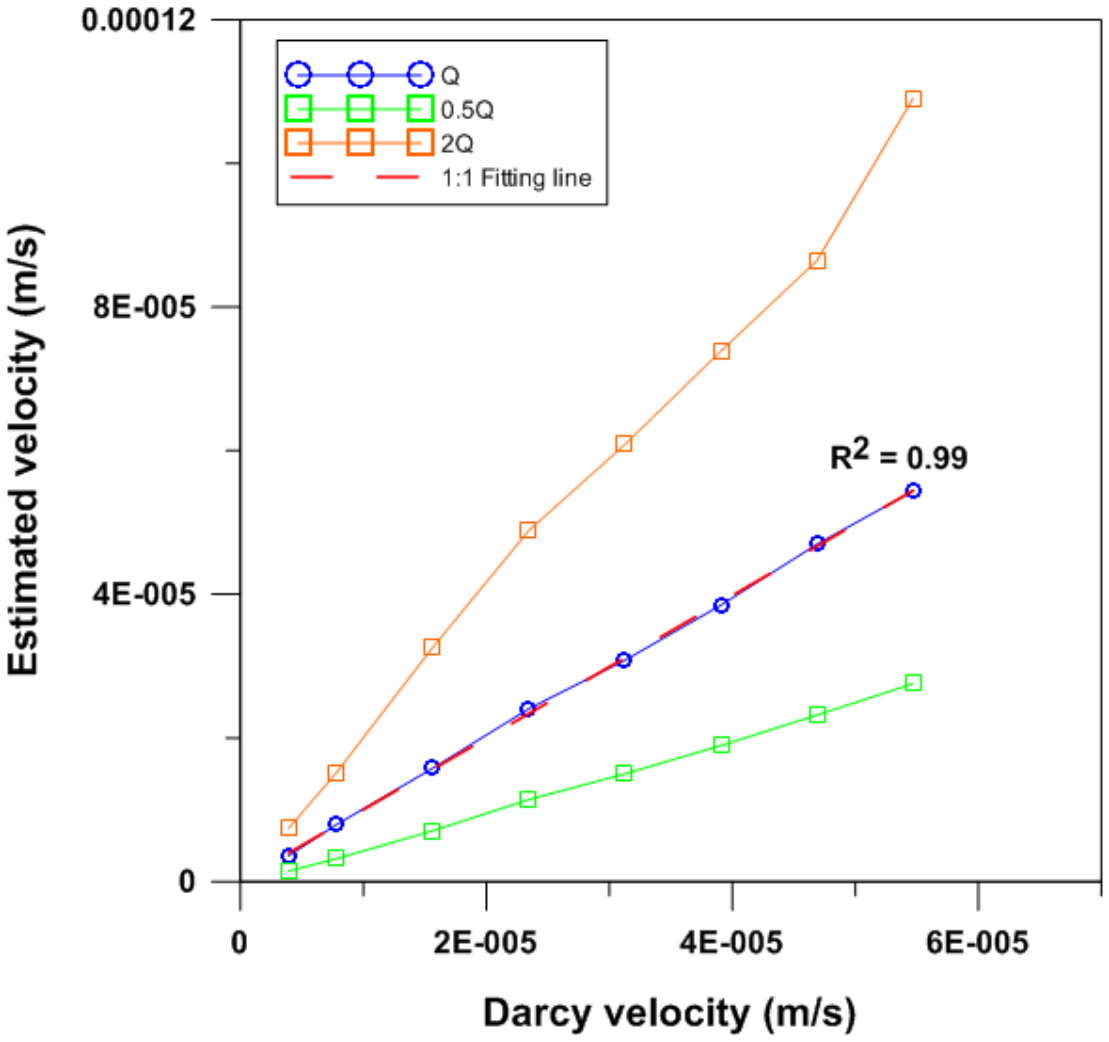

Fig. 3 - 22. The comparison of estimated velocity and Darcy velocity as applying higher (2Q) and lower (0.5Q) pumping rate.

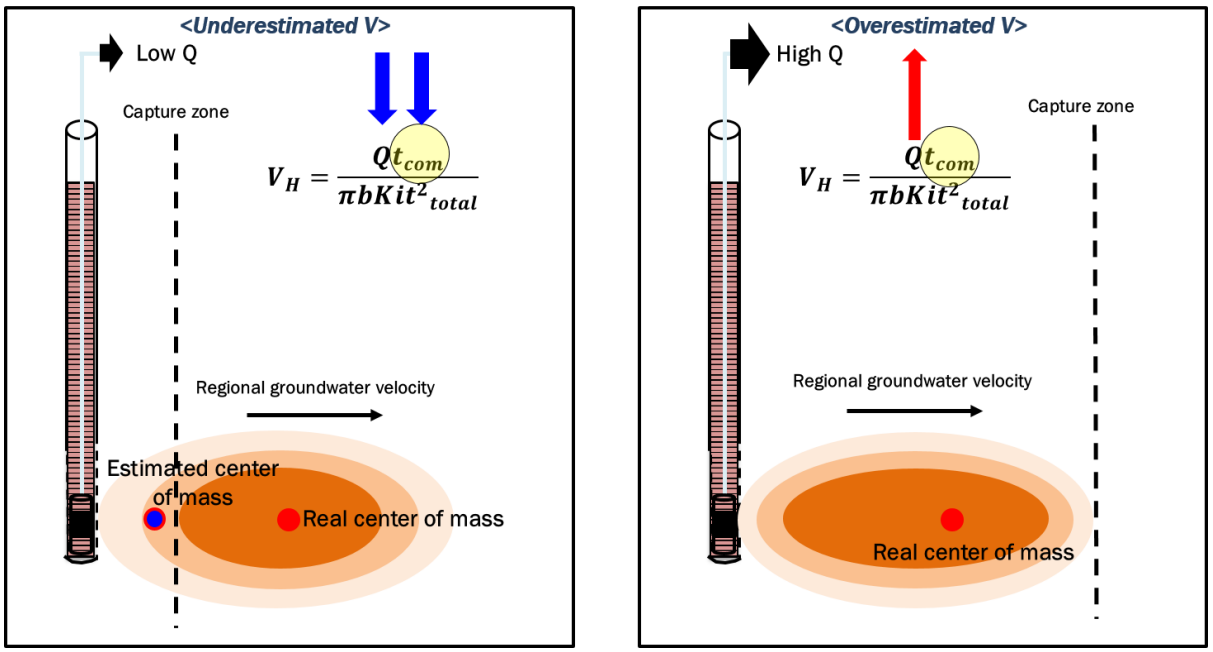

Fig. 3 - 23. The conceptual model of the effect of pumping rate on estimating linear velocity as applying low pumping rate (left) and high pumping rate (right)

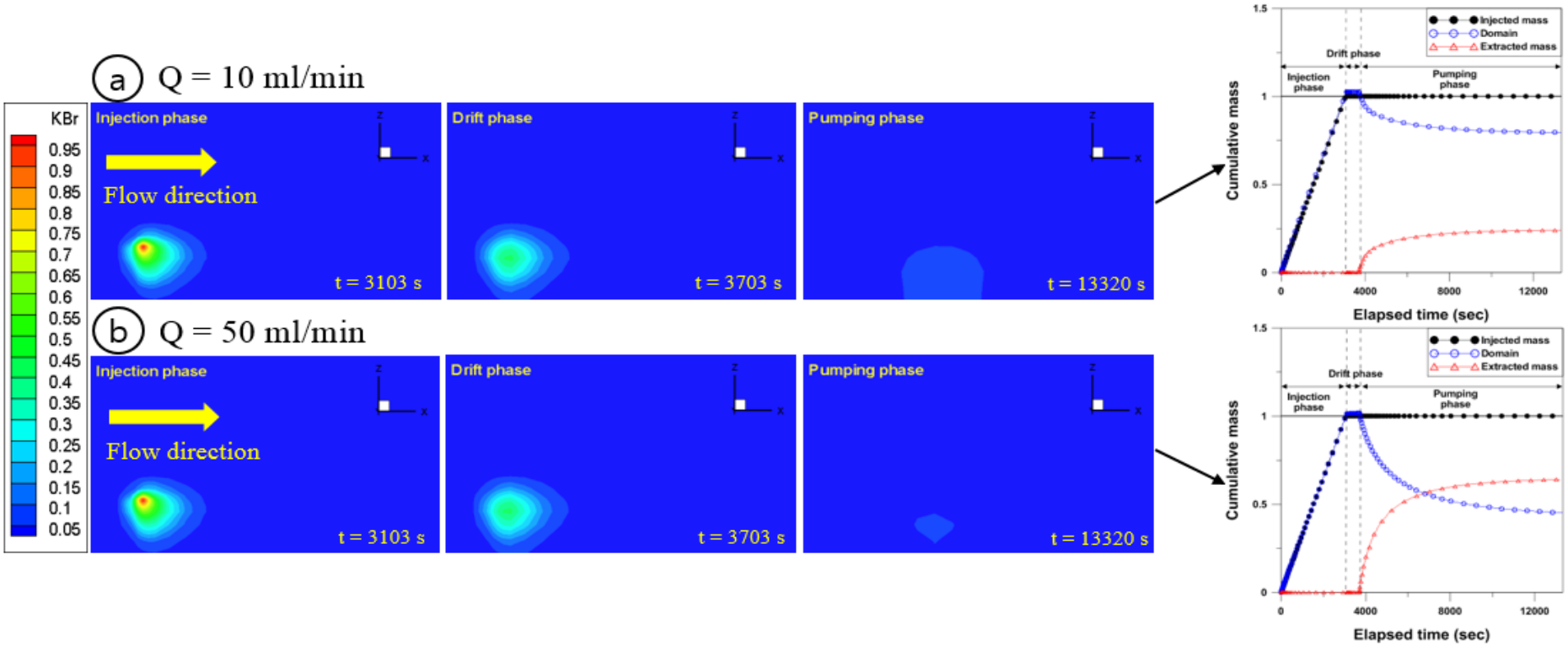

Fig. 3 - 24. Numerical simulation results in no-density effect condition (160 mg/L) at 3 time points (t = 3103 s: the end of injection phase, t = 3703 s: the end of drift phase, and t = 13320 s: the end of pumping phase) with the pumping rates of (a) 10 ml/min and (b) 50 ml/min.

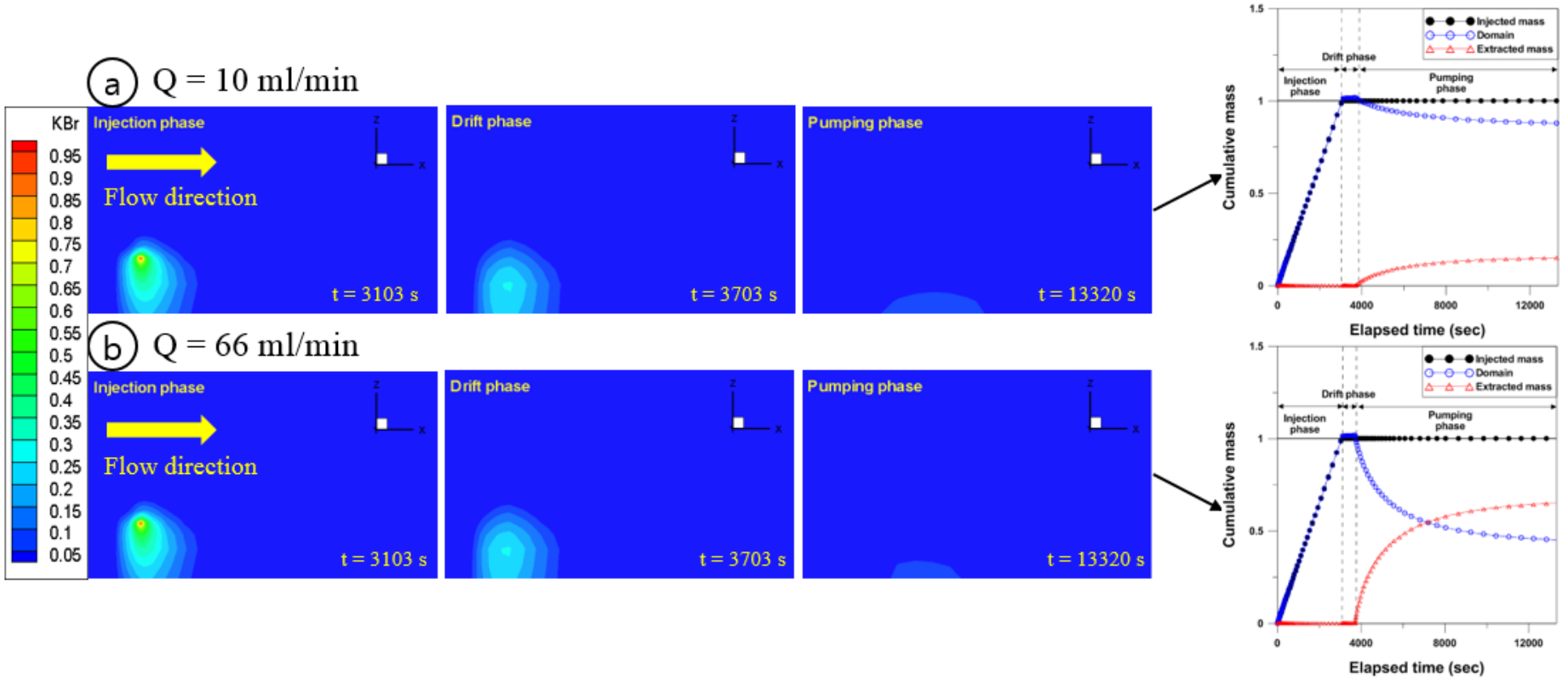

Fig. 3 - 25. Numerical simulation results in density effect condition (500 mg/L) at 3 time points (t = 3103 s: the end of injection phase, t = 3703 s: the end of drift phase, and t = 13320 s: the end of pumping phase) with the pumping rates of (a) 10 ml/min and (b) 66 ml/min.

4 CONCLUSIONS

In this study, single well push-drift-pull tracer tests were performed with field-scale and laboratory-scale experiments. The field-scale tests were performed focused on the application of single well push-drift-pull tracer test at CCS environmental monitoring site to characterize the hydrogeologic features of the study site. The environmental impact of CO_2 can be observed with properly installed monitoring wells near the injection point.

The major results obtained from field push-drift-pull tests can be summarized as follows:

1. The mass recovery percentage of tracers showed different values, depending on the property of tracers. The mass recovery percentage of salt tracer (non-volatile) was over 90 % and most of salt tracer was recovered. However, the recovery percentages of SF_6 (volatile) was less than 62%, which was lower than salt tracer. Furthermore, the recovery percentage of SF_6 was lowered as the drift time increased from Test 1-2 (1 day) to Test 2-1 (2 days). The reason of this mass recovery difference might by the degassing of the SF_6 gas tracer around the water table. Based on the results of field tests, the importance of groundwater monitoring as well as gas monitoring at the unsaturated zone was addressed. Therefore, an optimized monitoring network system in both saturated and unsaturated zones was installed for CO_2 water injection and leakage test.

2. The effective porosity of EIT site was estimated to be 0.02 - 0.07 and regional groundwater velocity was ranged from 0.21 m/d to 0.44 m/d. Based on these results, the effective CO_2 monitoring network system including an unsaturated zone was installed at the study site.

The laboratory-scale tests were performed focused on investigating the factors that might affect the results of push-drift-pull tests. Although it is known that many factors affect the result

of push-drift-pull tracer test, density effect and pumping rate have been rarely considered as important influential factors in evaluating linear velocity. The influence of density and pumping rate was estimated from the laboratory-scale experiments and numerical simulations. In addition, sensitivity analysis was carried out to identify the impact of several factors on tracer breakthrough curve. The factors tested in sensitivity analysis were drift time, density, hydraulic gradient, and well penetrating depth.

The major results obtained from laboratory-scale tests can be summarized as follows:

1. Drift time, density, and hydraulic gradient can affect the early part of breakthrough curve. It denotes that the sampling interval should be shortened at the early part of push-drift-pull test to obtain the peak point of breakthrough curve after changing the factors. However, test results showed that the difference of penetrating depth did not make much difference to the shape of breakthrough curve.

2. As the input tracer concentration was increased, the linear velocity was underestimated because density induced-sinking causes the underestimated horizontal travel distance. In addition, the reasonable pumping rate should be applied during pull phase of test. When the high pumping rate was applied the linear velocity was overestimated, and low pumping rate induces underestimated linear velocity because it causes the incorrect center of mass time (t_{com}).

5 REFERENCE

Addy, K., Kellogg, D.Q., Gold, A.J., Groffman, P.M., Ferendo, G., and Sawyer, C., 2002, In situ push-pull method to determine ground water denitrification in riparian zones, Journal of Environmental Quality, 31(3), 1017-1024.

Barth, G.R., Illangasekare, T.H., Hill, M.C., and Rajaram, H., 2001, A new tracer-density criterion for heterogeneous porous media, Water Resources Research, 37(1), 21-31.

Becker, M.W. and Shapiro, A.M., 2003, Interpreting tracer breakthrough tailing from different forced-gradient experiment configurations in fractured bedrock, Water Resources Research, 39(1), 1024.

Cahil, A.G., Marker, P., and Jakobsen, R., 2014, Hydrogeochemical and mineralogical effects of sustained CO2 contamination in a shallow sandy aquifer: A field-scale controlled release experiment, Water Resources Research, 50, 1735-1755.

Fetter, C. W., 1999, Contaminant hydrogeology, Vol. 500, New Jersey: Prentice hall.

Ghergut, I., Behrens, H., and Sauter, M., 2013, Single-well tracer push-pull test sensitivity to fracture aperture and spacing, Proceedings, Thirty-eighth workshop on geothermal reservoir engineering Stanford University, Stanford, California, February 11-13.

Grubb, S., 1993, Analytical model for estimation of steady-state capture zones of pumping wells in confined and unconfined aquifers, Ground water, 31(1), 27-32.

Haggerty, R., McKenna, S.A., and Meigs, L.C., 2000, On the late-time behavior of tracer test breakthrough curves, Water Resources Research, 36, 3467-3479.

Hall, S.H., Luttrell, S.P., and Cronin, W.E., 1991, A Method for estimating Effective Porosity and Ground-Water Velocity, Ground water, 29, 171-174.

Harvey, J.W., Wagner, B.J., and Bencala, K.E., Evaluating the reliability of the stream tracer approach to characterize stream-subsurface water exchange, Water Resources Research, 32, 2441-2451.

Hebig, K.H., Zeilfelder, S., Ito, N., Machida, Marui, A., and Scheytt, T.J., 2015, Study of the effects of the chaser in push-pull tracer tests by using temporal moment analysis, Geothermics, 54, 43-53.

Humez, P., Lagneau, V., Lions, J., and Negrel, P., 2013, Assessing the potential consequences of CO_2 leakage to freshwater resources: A batch-reaction experiment towards an isotopic tracing tool, Applied Geochemistry, 30, 178-190.

Hwang, H.T., 2004, Experimental and Numerical Sensitivity Analyses on Push-drift-pull Tracer Tests, Master's Thesis, Seoul National University, Korea.

IPCC (Intergovernmental Panel on Climate Change) (2005) Special report on carbon dioxide capture and storage, http://www.ipcc.ch.

IPCC (Intergovernmental Panel on Climate Change) (2007) Climate change 2007: the physical basis, the fourth assessment report of the intergovernmental panel on climate, summary for policymakers, http://www.ipcc.ch.

Istok, J.D., 2012, Push-pull tests for site characterization (Vol. 144), Springer Science and Business Media.

Kang, P.J., Kim, W.Y., and Lee, J.H., 1980, Manual of geologic map (Jincheon), Daejeon, Korea Institute of Geoscience and Mineral Resources. [in Korean]

Kharaka, Y.K., Cole, D.R., Hovorka, S.D., Gunter, W.D., Knauss, K.G., and Freifeld, B.M., 2006, Gas-water-rock interactions in Frio Formation following CO_2 injection: Implications for the storage of greenhouse gases in sedimentary basins, Geology, 34, 577-580.

Kharaka, Y.K., Thordsen, J.J., Kakouros, E., Ambats, G., Herkelrath, W.N., Beers, S.R., Birkholzer, J.T., Apps, J.A., Spycher, N.F., and Zheng, L., 2010, Changes in the chemistry of shallow groundwater related to the 2008 injection of CO2 at the ZERT field site, Bozeman, Montana, Environmental Earth Sciences, 60, 273-284.

Knopman, D.S., and Voss, C.I., 1987, Behavior of sensitivities in the one-dimensional advection-dispersion equation: implications for parameter estimation and sampling design, Water Resources Research, 23, 253-272.

Koo, C.M., Lee, K., Kim, M., and Kim, D.O., 2005, Automated System for Fast and Accurate Analysis of SF_6 Injected in the Surface Ocean, Environmental Science & Technology, 39, 8427-8433.

Leap, D.I. and Kaplan, P.G., 1988, A single-well tracing method for estimating regional advective velocity in a confined aquifer: Theory and preliminary laboratory verification, Water Resources Research, 24, 993-998.

Lee, K. K., Lee, S. H., Yun, S. T., and Jeen, S. W., 2016, Shallow groundwater system monitoring on controlled CO_2 release sites: a review on field experimental methods and efforts for CO_2 leakage detection, Geosciences Journal, 20, 569-583.

Lessoff, S.C., and L. F. Konikow, 1997, Ambiguity in measuring matrix diffusion with single-well injection / recovery tracer tests, Ground Water, 35(1), 166-176.

Ma, J., Wang, X., Gao, R., Zhang, X., Wei, Y., Wang, Z., Ma, J., Huang, C., Liu, L., Jiang, S., and Li, L., 2013, Monitoring the Safety of CO_2 Sequestration in Jingbian Field, Energy Procedia, 37, 3469-3478.

Meigs, L.C. and Beauheim, R.L., 2001, Tracer tests in a fractured dolomite: 1. Experimental design and observed tracer recoveries, Water Resources Research, 37, 1113-1128.

Myers, M., Stalker, L., Pejcic, B., and Ross, A., 2013, Tracers – Past, present and future applications in CO2 geosequestration, Applied Geochemistry, 30, 125–135.

Payne, F.C., Quinnan, J.A., and Potter, S.T., 2005, Remediation Hydraulics, CRC Press, NY, 276-282.

Peter, A., Hornbruch, G., and Dahmke, A., 2011, CO_2 leakage test in a shallow aquifer for investigating the geochemical impact of CO_2 on groundwater and for developing monitoring methods and concepts, Energy Procedia, 4, 4148-4153.

Peter, A., Lamert, H., Beyer, M., Hornbruch, G., Heinrich, B., Schulz, A., Geistlinger, H., Schreiber, B., Dietrich, P., and Werban, U., 2012, Investigation of the geochemical impact of CO_2 on shallow groundwater: design and implementation of a CO_2 injection test in Northeast Germany, Environmental Earth Sciences, 67, 335 – 349.

Shackelford, C.D., and Daniel, D.E., 1991, Diffusion in saturated soil. I: Background, Journal of Geotechnical Engineering, 117(3), 467-484.

Therrien, R., McLaren, R.G., Sudicky, E.A., and Panday, S.M., 2010, Hydrogeosphere: a three-dimensional numerical model describing fully-integrated subsurface and surface flow and solute transport, Groundwater Simulations Group, University of Waterloo, Waterloo, ON.

Trautz, R.C., Pugh, J.D., Varadharajan, C., Zheng, L., Bianchi, M., Nico, P.S., Spycher, N.F., Newell, D.L., Esposito, R.A., and Wu, Y., 2013, Effect of dissolved CO_2 on a shallow groundwater system: a controlled release field experiment, Environmental Science & Technology, 47, 298–305.

Zheng, L., Apps, J.A., Zhang, Y., Xu, T., and Birkholzer, J.T., 2009, Reactive transport simulations to study groundwater quality changes in response to CO_2 leakage from deep geological storage, Energy Procedia, 1, 1887-1894.

국문 초록

단공 주입양수 추적자 실험은 대수층의 특성을 파악하기 위해 사용되는 편리하고 경제적인 방법이지만 실험 결과가 다양한 실험 조건에 의해 영향을 받을 수 있다는 단점이 있다. 본 연구에서는 이산화탄소 저장 부지에서의 이산화탄소 누출 감지를 위한 효율적인 관측 관정 배치를 위하여 실제 이산화탄소 주입 전 주입양수 추적자 실험이 사용되었다. 또한, 실내 실험과 이를 바탕으로 한 수치 모의를 통해 실험 결과에 영향을 줄 수 있는 인자를 파악함으로써 좀 더 신뢰성 있는 결과를 얻기 위한 실험 설계를 할 수 있도록 하였다.

먼저, 현장에서의 두 가지 추적자(소금, SF_6)를 활용한 단공 주입양수 추적자 실험을 통해서 연구 부지에서의 국지적 규모 수리 특성(지하수 유속, 유효 공극률)을 도출해낼 수 있었다. 또한, 질량 회수율을 비교해 본 결과, 휘발성을 가지는 SF_6 추적자의 경우 비 휘발성의 소금추적자에 비해 낮은 질량 회수율을 보였으며, 이는 SF_6 추적자가 실험 간 진행된 탈기 과정으로 인한 것으로 생각되었으며 표류 시간을 더 늘렸을 경우 탈기가 더 많이 발생하는 것을 확인하였다. 실험으로 얻어진 수리 특성과 추적자 질량 회수율을 반영하여, 불포화대 관정을 포함하는 효율적인 관측 관정 네트워크를 구축할 수 있었다.

실내 실험에서는 실험 결과에 영향을 주는 인자를 파악하기 위해 대수층을 모의 구현하기 위한 수조 탱크를 활용하여 표류 시간, 추적자 밀도, 수리 경사, 관정 위치를 바꿔가며 일련의 실내 실험을 진행하였다. 실험을 통하여 얻어진 농도이력 곡선을 활용하여 시간에 따른 민감도 값을 계산할 수 있었으며, 이를 통하여 관정 위치 조건을 제외한 나머지 조건들을 변화시킬 경우 실험의 초반부에 샘플링 간격을 좀 더 조밀하게 하여 진행해야 좀 더 신뢰성 있는 농도 이력 곡선을 얻을 수 있다는 결론을 얻었다. 또한, 추적자의 밀도와 양수 속도가 선형 속도를 계산하는데 영향을 줄 수 있음을 알았으며 이에 대한 원인을 알아보기 위해서 수치 모의를 진행하였다. 그 결과, 주입되는 추적자 밀도가 증가할수록 수평 이동 거리가 짧아짐에 따라 선형 속도가 낮게 계산될 수 있음을 알 수 있었다. 또한, 양수 단계에서의 양수 속도에 따라 주입된 추적자

의 무게중심이 왜곡되어 계산됨에 따라 선형 속도가 과대평가 되거나 과소평가 될 수 있음을 알 수 있었다. 따라서 정확한 선형 속도 계산을 위해서는 적정 양수 속도가 적용되어야 한다는 결론을 얻을 수 있었다. 실내 실험 결과 본 실험에서 적용된 다양한 인자들을 고려한 단공 주입양수 실험 설계가 진행되어야 신뢰성 있는 실험 결과를 얻을 수 있음을 알 수 있었다.

주요어: 주입−표류−양수 추적자 실험, 다중 추적자 실험, 효율적인 이산화탄소 관측 네트워크, 추적자 실험 설계